

COMPOSITE HADRONS AND RELATIVISTIC NUCLEI\*

R. Blankenbecler  
Stanford Linear Accelerator Center  
Stanford University, Stanford, California 94305

(Lecture presented at Tübingen University, Tübingen, Germany, June 1977.)

---

\*Work supported by the Department of Energy

## I. INTRODUCTION

In these lectures I would like to describe a model of hadronic scattering at large momentum transfer, either transverse or longitudinal. This model emphasizes in this regime the importance of forces involving the interchange of constituents of the hadrons, hence the name, CIM, or constituent interchange model.<sup>1,2</sup> As will be shown, this model should not be thought of as being different from quark-quark scattering models, or from QCD (quantum chromodynamics) but contains both of them. Omission of the CIM diagrams is not a consistent approximation. The CIM is, in fact, a rearrangement of standard perturbation theory to take into account the fact that the binding force is very strong in color singlet states. We could call this Singlet Dominance. For example, if one demands that an anti-quark, or  $\bar{q}$ , be found a large distance from the center of a baryon, the easiest way for it to propagate to such distances is via intermediate states involving light mesonic (singlet) states. But more of this later on when the CIM contributions and their absolute normalization will be discussed.

Before discussing the physically complicated case of hadrons, it is helpful to discuss constituent models in a regime where we know they must apply—i. e. nuclear scattering.<sup>3</sup> In addition to developing our intuition and methods of approximation, we can extend the usual description of nuclei into the relativistic domain—that is, a regime where particle production occurs but does not dominate, where the finite size of nucleons plays an important role, and where the motions of the nucleons must be described by relativistic kinematics. All of this is clearly possible to include in a theoretical model but the important point is its simplicity and usefulness, and the ease with which predictions can be made. We will find a remarkably simple model that works quite well for certain experimental cross sections. Further tests are required before its general validity can be assessed.

## II. THE HARD SCATTERING EXPANSION

For applications to both the hadronic and nuclear case, an expansion of the full scattering amplitude must be made in order to compute anything. In the hadronic case the relevant expansion is called the hard scattering expansion, whereas in the nuclear case it is called the impulse approximation. Let us review some of the basic assumptions used in this familiar expansion. This is particularly important since by trying to add ad hoc features to the first term, it is possible to define nonsense that doesn't appear to be nonsense at first glance.

The hard scattering expansion for an inclusive reaction is illustrated in Fig. 1 and written as <sup>2</sup>

$$E_C \frac{d\sigma}{d^3C} (AB \rightarrow CX) = \sum_{a,b,d} \int dx d^2k_T dy d^2\ell_T G_{a/A}(x, k_T) G_{b/B}(y, \ell_T) r(s, s^1, x, y) E \frac{d\sigma}{d^3C} (ab \rightarrow Cd; s^1, t^1, u^1), \quad (2.1)$$

where the a, b, d sum is over incoherent final states. If this is the case, then the formula takes on a simple probabilistic meaning. The ratio  $r = \lambda(s^1, k_\mu^2, \ell_\mu^2) / xy \lambda(s, A^2, B^2)$  is the ratio of the internal (off shell) and external (on shell) phase space factors and  $\lambda(s, t, u)$  is the usual quadratic form,

$$\lambda(s, t, u) = s^2 + t^2 + u^2 - 2(st + su + tu).$$

If one keeps  $k_T$  and  $\ell_T$  small, one finds  $r \cong 1$ .

Our discussion will be based in the diagram shown in Fig. 1, which represents the inclusive process  $A+B \rightarrow C+X$ . Here the interaction takes place through the emission of virtual subsystems (a and b), which are the ones that scatter in an internal basic process  $a+b \rightarrow C+d$ , where C is the detected particle.  $M_0$  is the amplitude for this basic interaction, and the amplitudes for the emission of the

a and b subsystems will be contained in distribution functions  $G(x, \vec{k}_T)$ , to be defined precisely in a moment. However, the interpretation of the various factors in Eq. (1) is clear. The factor  $G_{a/A}(x, \vec{k}_T)$  is the probability of finding a constituent of type a in nucleus A with fractional "momentum" x and transverse momenta  $\vec{k}_T$ . A similar interpretation holds for  $G_{b/B}$ . The basic cross-section factor that actually produces the detected particle C also has a clear probabilistic meaning. We have neglected any final state decay to C for simplicity, but such can easily be added in.

The sum over the intermediate and final states must be chosen so that Eq. (2.1) is a sum over incoherent final states. This means that the simplest way to classify the terms is according to the final state configuration of particles, not the possible intermediate states that can contribute. The sum over a, b, and d must be chosen with the final state configurations in mind. For example, this means that one particular Feynman graph contributes to several terms in the sum depending upon the disposition of the final state particles, that is which particular particle (or particles) is recoiling against the large (transverse) momentum of particle C, for example.

The internal amplitude  $M_0$  that describes the process  $ab \rightarrow Cd$  must be predicted by the model or fit to experiment (as in the nuclear case).

The "momentum" fraction x (and y) is not exactly the momentum fraction of component a in A. It is defined rather as an "infinite" momentum fraction  $x = (a_0 + a_z)/(A_0 + A_z)$ . In detail, we define the awkward looking momenta

$$\begin{aligned}
 A &= \left( P_1 + \frac{A^2}{4P_1}, \vec{O}_T, P_1 - \frac{A^2}{4P_1} \right) \\
 B &= \left( P_2 + \frac{B^2}{4P_2}, \vec{O}_T, -P_2 + \frac{B^2}{4P_2} \right)
 \end{aligned}
 \tag{2.2}$$

where a particle's name and four-momentum are denoted by the same symbol except for the off-shell particles a and b. A and B have been defined in a general set of frames along the interaction axis. A specific frame in this set is selected by relating  $P_1$  and  $P_2$ . For example, the center-of-mass frame is defined by the conditions

$$P_1 - \frac{A^2}{4P_1} = P_2 - \frac{B^2}{4P_2}$$

and

$$\sqrt{s} = P_1 + \frac{A^2}{4P_1} + P_2 + \frac{B^2}{4P_2} .$$

The other momenta that are on-shell are defined as

$$\alpha = \left( (1-x)P_1 + \frac{\alpha^2 + k_T^2}{4(1-x)P_1} , -\vec{k}_T , (1-x)P_1 - \frac{\alpha^2 + k_T^2}{4(1-x)P_1} \right) \quad (2.3)$$

$$\beta = \left( (1-y)P_2 + \frac{\beta^2 + \ell_T^2}{4(1-y)P_2} , -\vec{\ell}_T , -1(-y)P_2 + \frac{\beta^2 + \ell_T^2}{4(1-y)P_2} \right)$$

This rather cumbersome set of variables will greatly simplify our later discussion. For example, note that with these parametrizations, the phase space integrals are of the form

$$d^4\alpha = d^2k_T \frac{dx}{2|1-x|} d\alpha^2$$

and then the  $\alpha^2$  integral, due to the corresponding on-mass-shell  $\delta$ -function, is trivial. The off-shell momenta are calculated by momentum conservation:

$$\begin{aligned} a &= \left( xP_1 + \frac{k^2 + k_T^2}{4xP_1} , \vec{k}_T , xP_1 - \frac{k^2 + k_T^2}{4xP_1} \right) \\ b &= \left( yP_2 + \frac{\ell^2 + \ell_T^2}{4yP_2} , \vec{\ell}_T , -yP_2 + \frac{\ell^2 + \ell_T^2}{4yP_2} \right) , \end{aligned} \quad (2.4)$$

where

$$\begin{aligned} k^2 &= \left( x(1-x)A^2 - x\alpha^2 - k_T^2 \right) / (1-x) \\ \ell^2 &= \left( y(1-y)B^2 - y\beta^2 - \ell_T^2 \right) / (1-y). \end{aligned} \quad (2.5)$$

Note that with these parametrizations, as mentioned before,

$$x = \frac{a_0 + a_3}{A_0 + A_3}$$

which is the usual light-cone variable, and hence  $x$  can only have values between zero and one.

Since the  $G$ 's are probability functions, they must be related to the square of a wave function; a careful analysis shows that

$$G_{a/A}(x, \vec{k}_T) = \frac{1}{2(2\pi)^3} \frac{x}{(1-x)} |\psi(x, \vec{k}_T)|^2 \quad (2.6)$$

where  $\psi$  is the bound state Bethe-Salpeter wave function with one leg ( $\alpha$ ) on-shell. We will see in our analysis that the distribution functions are explicitly measured in the experiments we are considering. For this reason it is important to have a reasonably good prediction or description of their properties. We shall analyze these functions in detail and get information about them from limiting cases, like the non-relativistic limit and the short distance or ultrarelativistic behavior.

It is also straightforward to derive an equation for the electromagnetic form factor of the state  $A$  in terms of  $\psi$  and the result is

$$F_A(q_T^2) = \sum_a F_a(q^2) \int \frac{dx d^2k_T}{2(2\pi)^3} \frac{x}{(1-x)} \psi^*(x, \vec{k}_T) \psi(x, \vec{k}_T - (1-x)\vec{q}_T) \quad (2.7)$$

where the integral multiplying  $F_a$  is the body form factor of the nucleus. This can be used to predict the form factor when a sufficiently promising wave function  $\psi(x, k_T)$  is developed. We are particularly interested in possible relations between the large  $q_T^2$  behavior of the form factor and inclusive measurements in the forward direction.

### III. INCOHERENCE PROBLEMS

Let us illustrate some of the problems associated with keeping the various terms in Eq. (2.1) incoherent. For simplicity, we shall consider the production of a massive lepton pair (the Drell-Yan process) since the gauge invariance of the photon more or less forces us to a consistent treatment.<sup>4</sup> In QCD, the gauge invariance with respect to the gluons will certainly force one to a similar complete treatment with similar results.

Consider the two diagrams in Fig. 2 which correspond to  $a=\bar{q}$ ,  $b=q$ , and  $b=(qq)$ , respectively. The first diagram is the natural one in the Drell-Yan theory<sup>5</sup> in order to produce large  $Q_T$  pairs. The large transverse momentum of the pair arises from the wave function or structure function  $G_{q/p}(y, \ell_T)$ . However, this is an incorrect treatment since the second  $b=(qq)$  term is coherent with the first and is even of the same order in all couplings. It is necessary to treat these two terms together and to include them both. They can be described as an initial and a final state interaction, respectively. From the relevant quark's point of view, they are the direct and crossed graph for the process  $\text{glue} + \text{quark} \rightarrow \text{photon} + \text{quark}$ . At large  $Q_T$ , one finds that these two terms cancel to leading order, as will be discussed in more detail later.

That this is not an unexpected feature of initial and final state interactions can be seen by considering the theorem derived in potential scattering by Amado and Woloshyn.<sup>6</sup> They proved that the term with the leading behavior of the wave function at large relative momentum actually cancels in a general class of break-up reactions. This cancellation is due (essentially) to the orthogonality of the bound and (ingoing) scattering states and is therefore expected to be a very general phenomena.

We have seen therefore that simply adding a large  $k_T$  spectrum to the initial state quarks and then using the Drell-Yan formula is incorrect in principle. This should come as no surprise since D-Y stated in their original paper that their model was not gauge invariant if large transverse momenta were allowed. It is easy to see that if an intermediate quark carries a large  $k_T$ , its  $(\text{mass})^2$  is of order  $(-k_T^2/(1-x))$ . Thus it is not possible to make such a contribution gauge invariant to this order unless the photon is attached to both ends of this far offshell propagator. This leads us naturally to the initial and final state interaction effects described earlier. One way to avoid troubles here is to demand that the intermediate particles a and b remain near their respective mass shells and hence that they not carry a large transverse momentum. This forces all large momentum transfers to occur in the central process. This in turn allows the photon to be attached in all necessary orderings to insure gauge invariance, as well as the proper incoherence properties of the hard scattering expansion.

We discussed final state photons above only because a proper treatment of gauge invariance forces us to a reasonable result. The same is true of reactions in which ordinary particles are produced — one must still satisfy the conditions used to define the hard scattering expansion. This is especially true in QCD where the gluons must be treated in a gauge invariant manner. Since we are now forewarned, let us return to a treatment of nuclear (or heavy-ion) scattering processes.

#### IV. NUCLEAR WAVE FUNCTIONS AND COUNTING RULES

We shall demand that our theory join onto the familiar nonrelativistic treatments when the energies and momenta are small. In particular, the  $G$  function must be closely related in this limit with the square of the nonrelativistic wave function. This requirement will allow us to achieve a clearer understanding of these functions and their expected behavior, and also to explore the way masses should enter into our formalism.

First we want to see the meaning of the  $x$ -variable in a nonrelativistic limit. For momenta small with respect to the masses, and in the rest frame of the nucleus,  $x$  becomes

$$x \simeq \frac{a}{A} + \frac{k_z}{A} \quad , \quad (4.1)$$

and hence is related to the longitudinal momentum, measuring deviations with respect to a central value  $\frac{a}{A}$ . Since on the average, and in the rest frame of the nucleus, we expect  $k_z = 0$ , this means that on the average  $x = \frac{a}{A}$ . In other words, each nucleon carries the same fraction of the total momentum of the nucleus. A very reasonable result in the weak binding limit.

Recall that  $G$  is the probability of finding a constituent of  $A$  with longitudinal momentum  $x$  and transverse momentum  $\vec{k}_T$ . This means that  $G$  must have a maximum at  $x \simeq \frac{a}{A}$  (the average nucleon longitudinal momentum) and at  $\vec{k}_T = 0$ . Considering the definition of  $G$ , and using the Bethe-Salpeter equation we see that

$$G \sim \frac{\phi^2 x(1-x)}{\left[ k_T^2 + M^2(x) \right]^2} \quad , \quad (4.2)$$

where  $\phi$  is defined as the vertex function and

$$M^2(x) = (1-x)(a^2 - k^2) - k_T^2 = (1-x)a^2 + x\alpha^2 - x(1-x)A^2 \quad .$$

This form implies that G has a maximum at  $\vec{k}_T=0$  and at  $x=x_0$ , where  $M^2(x)$  is a minimum. We find

$$x_0 = \frac{A^2 + a^2 - \alpha^2}{2A^2} \cong \frac{a}{A} , \quad (4.3)$$

and as expected, the constituents prefer to share the momentum according to their mass.

In the limit of small momenta one then finds

$$k_T^2 + M^2(x) \cong 2a\epsilon \left( \frac{A-1}{A} \right) + \vec{k}^2 \quad (4.4)$$

where it has been assumed that the binding energy for nucleon  $\epsilon$  is the same for both A and  $\alpha$ . The G function becomes

$$G \sim |\psi_{NR}(\vec{k})|^2 \sim \frac{\phi_{NR}^2(\vec{k})}{[a\epsilon + \vec{k}^2]^2} ,$$

where (A=2 for simplicity)

$$\phi_{NR}^2 \sim x_0(1-x_0)\phi^2 .$$

In order to have a better understanding of the function  $\phi_{NR}$ , consider the Schrodinger equation in momentum space

$$\psi_{NR}(\vec{k}) = (a\epsilon + \vec{k}^2)^{-1} \int d^3p V(\vec{k} - \vec{p}) \psi_{NR}(\vec{p}) = (a\epsilon + \vec{k}^2)^{-1} \phi_{NR}(\vec{k}) ,$$

so that the vertex function expresses more or less directly the behavior of the potential V. The falloff of  $\phi$  is related to the softness (or hardness) of the potential. As a simple example consider a general Hulthen model of the nuclear wave function:

$$\psi_{NR} = (a\epsilon + \vec{k}^2)^{-1} (a\epsilon_1 + \vec{k}^2)^{\frac{1-g}{2}} .$$

In the familiar Hulthen deuteron case, one usually chooses  $g=3$ , and  $\epsilon_1 \sim 36\epsilon$ . The second factor is then much flatter in  $\vec{k}^2$  than the first.

A relativistic version of this wave function can be achieved by writing

$$\psi = \frac{N(x)}{(k^2 - a^2) \frac{g-1}{(k_1^2 - a_1^2)^2}}, \quad (4.5)$$

where  $N(x)$  is slowly varying for  $x$  near 1, and where we choose

$$(1-x)(a_1^2 - k_1^2) = M^2(x) + \delta^2 + k_T^2 \quad (4.6)$$

since the second factor should have a minimum at the same place as the first, i. e.  $x=x_0$ .

The form factor for the type of wave function of (4.5) is easily seen to fall as

$$F^2 \left( q_T^2 \right) \sim \left( q_T^2 \right)^{-g-1} \quad (4.7)$$

for large  $q_T^2$ . Thus the falloff of the form factor and the behavior of  $G$  for large  $k_T^2$  are closely related and also we shall see that the behavior of  $G$  for  $x$  near 1 is also closely related to the form factor falloff. This latter relation is the Drell-Yan-West relation.

For general  $x$ , the relativistic  $G$  function can then be written as

$$G(x, \vec{k}_T) = \frac{N^2(x) x(1-x)^g}{2(2\pi)^3} \left[ M^2(x) + k_T^2 \right]^{-2} \left[ M_1^2(x) + k_T^2 \right]^{1-g}. \quad (4.8)$$

For  $x \simeq x_0$ , the denominator factors are rapidly varying and as has been discussed, this reduces to a familiar nonrelativistic Hulthen form. For  $x \gg x_0$ , the numerator factors control the behavior of  $G$ , and

$$G(x, \vec{k}_T) \sim (1-x)^g$$

while its large  $k_T^2$  behavior is  $(k_T^2)^{-g-1}$ .

In our analysis, the behavior of  $G$  for  $x \gg x_0$  will be especially important. Note that this is new information not directly contained in the nonrelativistic wave function. We can also discuss quasielastic scattering which explores the  $G$  function for  $x \sim x_0$  as well. Let us now turn to a discussion of the calculation of the power  $g$  in selected theories of the nucleon-nucleon interaction.

Our main contact with experimental data is through the structure functions  $G(x, k_T)$ . A helpful tool for expressing the predictions of specific theories is in terms of "counting rules." <sup>7,8</sup> These allow one to characterize the asymptotic behavior of  $G$  in terms of the number of constituents and the short distance behavior of the basic interactions of the theory.

The procedure here is to extract the leading behavior from the lowest order diagram in perturbation theory. For "soft" theories, one can show that the higher orders either are small compared to the leading term or have the same behavior. Consider the wave function (or structure function) diagram given in Fig. 3, where  $k$  is the momentum of particle  $a$  and is defined in Eq. (2.4). We shall assume scalar particles for simplicity. Note that  $A$  now also means the atomic number of particle  $A$ .

For a renormalizable interaction between the constituents, such as vector exchange with point interactions, the falloff of the vertex function arises solely from the constituent propagators. One finds

$$\phi \sim \left(k_1^2 - a_1^2\right)^{1-n} .$$

where the masses in  $k_1$  (see Eq. (II-15)) depend on detailed properties of the force. The wave function is

$$\psi \sim \left(k^2 - a^2\right)^{-1} \left(k_1^2 - a_1^2\right)^{1-n}$$

Comparison with Eq. (II-14) immediately tells us that

$$g = 2A - 3$$

As a perhaps more relevant example, consider a nucleon-nucleon interaction mediated by the exchange of vector mesons, such as rhos or omegas, with a monopole form factor at each vertex (vector dominance would assume such a behavior to fit the dipole nucleon form factor). One finds

$$\phi \sim \left(k_1^2 - a_1^2\right)^{1-n} \left(k_2^2 - a_2^2\right)^{-2n}$$

where the masses in the form factors and/or gluon propagators are chosen to be the same for simplicity. The final result in this case is

$$g = 6A - 7 \quad .$$

This is the same result as one would get by counting quarks. While one might expect that the quark degrees of freedom become relevant at ultrahigh energies where they can be excited, we see that one gets the same prediction for  $g$  in this theory when the nucleon form factor effects play a role. These, of course, may in turn be due to internal structure, but the internal degrees of freedom need not be fully excited.

For more general structure functions  $G_{a/A}$ , where the state  $a$  is a bound state of  $a$  nucleons, a similar analysis can be carried through. One finds in this case

$$g = 2T(A-a) - 1 \tag{4.9}$$

where  $T$  ( $= 1, 3, \text{ etc.}$ ) depends upon the basic nucleon-nucleon interaction as discussed earlier. Again, we have assumed full breakup of the nucleus after  $a$  is extracted. If the nucleus is not fully broken up, then the calculation is extremely complicated but one might conjecture that  $g$  should be replaced by

$$g = 2T(A-a)_{\text{eff}} - 1 \quad , \tag{4.10}$$

where  $(A-a)_{\text{eff}}$  is the effective number of fragments that the remaining nucleons produce. One may also expect additional nonscaling behavior as well if some of the fragments remain bound.

Now we shall predict the behavior of inclusive yields in order to test the theory and to see if one value of  $T$  fits all the inclusive scattering reactions and the elastic form factors.

## V. INTERACTION BETWEEN NUCLEI

As a first application we will consider inclusive scattering of nuclei at high energies and get simple predictions that can easily be compared with experiment without extensive numerical calculation.<sup>3</sup> First, consider the situation in which the energy per nucleon is large compared to the nucleon mass. The kinematics for this regime is quite simple:

$$\begin{aligned}
 s' &= xys \\
 t' &= yt \\
 u' &= xu \\
 d^2 &= xys + yt + xu
 \end{aligned}
 \tag{5.1}$$

and

$$C_T^2 = \frac{ut}{s} = C_T'^2$$

The condition  $d^2 > 0$  restricts the range of  $x$  and  $y$  that contribute for fixed values of  $s$ ,  $t$ ,  $u$ , and all finite masses have been neglected. Note that the internal reaction can be inclusive ( $d^2 > 0$ ) or exclusive ( $d^2 = 0$ ). This last situation is also called quasielastic scattering.

All inclusive basic processes of interest to us here will be parametrized as

$$\left[ E_C \frac{d\sigma}{d^3C} \right]' = E(s') \int \delta^3(\mathbf{x}'_F) \int f(k'_T)
 \tag{5.2}$$

and exclusive processes as

$$\left[ E_C \frac{d\sigma}{d^3C} \right]' = E(s') \delta \left[ (k+l-C)^2 - d^2 \right] f(k'_T)
 \tag{5.3}$$

where  $k'_T = C_T - k_T - l_T$  and  $E(s')$  is assumed slowly varying.  $H$  will be assumed to be constant. The function  $f(k'_T)$  is strongly peaked at  $k'_T = 0$  (for small  $k'_T$  it could be written as an exponential  $e^{-r^2 k'^2_T}$ , for example).

Now we will go into a discussion of our model in some regions of phase space in which it is easy to get predictions.

First define in terms of the missing mass  $m$

$$\begin{aligned} \epsilon &= \frac{m^2}{s} = 1 - x_R \cong 1 - \frac{|\vec{C}_{cm}|}{|\vec{C}_{max}|} \\ x_T &= \frac{C_T}{C_{max}} \\ x_L &= \frac{C_L}{C_{max}} \cong \frac{t-u}{s} \quad , \\ x_R &= \sqrt{x_T^2 + x_L^2} \end{aligned} \quad (5.4)$$

and for the most part we will concentrate in the region  $\epsilon$  not near one.

When  $t$  is fixed (and  $s, u$  large), one finds ( $x_R = x_F$ , Feynman's variable) in this the projectile fragmentation region,

$$1 - x'_F = 1 + \frac{yt + xu}{xys} \quad ,$$

and hence  $x'_F \cong x_F/y$ . The condition  $d^2 > 0$  becomes  $y > x_F$ . In this regime, the inclusive cross section becomes

$$\sum_{ab} \int_0^1 dx d^2 k_T G_{a/A}(x, \vec{k}_T) \int_{x_F}^1 dy d^2 l_T G_{b/B}(y, \vec{l}_T) \left[ E_C \frac{d\sigma}{d^3 C} \right] \quad . \quad (5.5)$$

First consider an inclusive basic process. Since  $f(\vec{k}_T)$  in formula (III-2) is strongly peaked in  $k_T^2$ , we can approximate the  $k_T$  and  $l_T$  integrals by replacing  $k_T^2$  and  $l_T^2$  in the  $G$ 's by the mean value  $K^2$  which should be of the order of  $C_T^2$ .

The inclusive cross section is then proportional to

$$\propto \int_{x_F}^1 dy \frac{N^2(y) y(1-y)^{g_B}}{\left[ K^2 + M^2(y) \right]^2 \left[ K^2 + M_1^2(y) \right]^{g-1}} (1-x_F/y)^H \quad .$$

Note that the distribution for the target  $G_{a/A}$  has integrated out in this limit, and it depends on A through its normalization only.

If  $C_T^2 \gtrsim M_1^2(x_0)$ , and if  $x_F$  is not small compared to  $x_0$ , then the main variation in the integrand is from the factors of  $(1-y)$  and  $(1-x_F/y)$ . The first factor cuts off the integrand near  $y = 1$  and the other near  $y = x_F$ . If only their variation is retained, and the denominators taken constant, we have

$$E \frac{d}{d^3 C} \sim (1-x_F)^{g_B+H+1} . \quad (5.6)$$

A more accurate treatment is possible but the above will suffice for our purposes.

In the target fragmentation region, where  $u$  is fixed and  $s, t$  large, the above arguments can be repeated with the result that

$$\sim (1+x_F)^{g_A+H+1} , \quad (5.7)$$

where  $g_A$  is the power behavior of the target distribution function  $G_{a/A}$ . This result could also have been achieved by simply interchanging the target and beam particles in the previous result. These predictions will be compared to data in a later section.

One can estimate the range of validity in  $x_F$  of the above formulas by a simple argument. The momentum fraction  $x_F$  must be large enough so that the particle is out of the "quasielastic" peak where the denominator factors in Eq. (III-6) are rapidly varying. The average momentum fraction  $x_B$  of particle B is  $\langle x_B \rangle = 1/B$ . The average  $x$  retained by the detected particle is roughly  $\simeq 1/(H+2)$ . Therefore, the behavior given by Eq. (5.6) should hold reasonably well for  $x_F \gtrsim 1/B(H+2)$ .

For an exclusive basic process, which yields the familiar quasielastic formula, the calculation is also simple. Using Eq. (III-3) and expanding the arguments of the delta function for the case  $b+n \rightarrow C+n$ , where  $b$  and  $C$  are nucleons, one finds that a reasonable approximation is:

$$\left[ E \frac{d\sigma}{d^3C} \right]' = E(s') \delta \left[ x(s-A^2-B^2)(x_F - \Delta - y) \right] f(k_T')$$

where the shift  $\Delta$  has to be calculated using more exact kinematics. At high energies  $\Delta \rightarrow 0$ ; for the experimental data to be discussed shortly,  $\Delta \sim 0.06$ .

Again the  $x$  integral is not restricted and the full inclusive cross section is

$$E \frac{d\sigma}{d^3C} \sim G_{C/B} \left( x_F - \Delta, K^2 \right) \left( \frac{d\sigma}{dt} \right)' , \quad (5.8)$$

where the prime means that the elastic cross section is evaluated at reduced kinematics. Thus, the quasielastic peak should occur at  $x_F = C/B + \Delta$ . This is slightly larger than the naive expectation  $C/B$ , the most likely momentum in the state B. This shift will be included in all our numerical calculations. Eq. (5.8) can be interpreted as a relativistic generalization of the Glauber approximation but with a more precise definition of the covariant wave function.

For our particular model, we require, of course, that the same value of  $T$  fit both the inclusive (say pion production) and exclusive case.

Another situation in which we can get simple predictions from the model is when the produced particle (C) has large transverse momentum ( $s, t, u$  large, and masses negligible). In this regime ( $\theta_{cm} \cong 90^\circ$ ), we have that

$$x_L \cong 0$$

$$x_R \cong x_T$$

and

$$1 - x_R' \cong \frac{d^2}{s'} = \frac{x_T}{2} \left( \frac{1}{x} + \frac{1}{y} \right) . \quad (5.9)$$

Inclusive basic process. The condition  $d^2 > 0$  means that in the limit of primary interest to us  $x$  and  $y$  in formula (II-7) are going to be both close to one. By a similar analysis as in Section A, the  $\vec{k}_T$  and  $\vec{\ell}_T$  can then be integrated out and we can write approximately ( $G(x) \sim (1-x)^g$ )

$$\sim \int_0^1 dx \int_0^1 dy (1-x)^{g_a} (1-y)^{g_b} \left[ R'_C(a+b \rightarrow C+X) \right] \theta(d^2) ,$$

which can be applied, for example, to pion and proton (not including the quasi-elastic peak) production at large transverse momentum.

We will consider two different parametrizations for the internal cross section:

$$\sim (1-x'_R)^H f(C'_T{}^2) s^P$$

and then one finds, using Eq. (III-12):

$$E_C \frac{d\sigma}{d^3C} \sim \epsilon^{F+H+1} (C_T^2)^P f(C_T^2) , \quad (5.10)$$

where  $F = 1 + g_a + g_b$  and where  $\epsilon$  is close to zero. For  $\epsilon$  not near zero, there is a function which is slowly varying in  $\epsilon$  that multiplies this result.

We see that this regime gives us information about the distribution functions of both target and projectile. It also follows that the  $C_T^2$  dependence is the same for the complete process as it is for the internal interaction, except for the  $(C_T^2)^P$  factor, but  $P$  is normally small and this factor is essentially constant.

In certain cases (quasielectric scattering), the internal basic process is going to be dominated by elastic scattering. This means that the cross section can be written as  $(G(x) \sim (1-x)^g)$

$$\int_0^1 dx \int_0^1 dy (1-x)^{g_a} (1-x)^{g_b} \left[ R'_C(C+b \rightarrow C+d) \right] ,$$

where  $R'_C = \delta(d^2) \frac{s'}{\pi} \frac{d\sigma}{dt} (C+b \rightarrow C+d)$  and  $R'_C$  now contains a factor  $\delta(d^2)$ .

Writing the elastic cross section as

$$\frac{d\sigma}{dt} \sim s'^P f(C_T^2)$$

gives the prediction

$$E_C \frac{d\sigma}{d^3C} = I(\epsilon) \epsilon^F (C_T^2)^P f(C_T^2) . \quad (5.11)$$

Note that in this case the multiplying function  $I(\epsilon)$  must be rapidly varying in order to produce the quasielastic peak. Right at the quasielastic peak we have  $\langle y \rangle \simeq 1/B, \langle x \rangle \simeq 1/A$ , where A and B are the atomic number of the states A and B respectively. Using  $d^2 = 0$ , we get for the peak value (neglecting kinematic mass effects)

$$\epsilon_Q \simeq 1 - \frac{2}{A+B} .$$

One expects that  $(I(\epsilon) \epsilon^F)$  will be rapidly varying and will lead to a quasielastic peak for  $\epsilon \sim \epsilon_Q$ . For  $\epsilon > \epsilon_Q$ ,  $I(\epsilon)$  should vary much less, and the main  $\epsilon$  dependence should come from the  $\epsilon^F$  factor.

In the previous section we have presented a detailed analysis of our relativistic model and the predictions it gives when applied in specific regions of phase space (projectile fragmentation, target fragmentation and large  $p_T$ ). While because of their simplicity we have considered only these special cases, it is possible to obtain a generalization of these results that is valid for all angles. In fact, it can be shown that

$$E_C \frac{d\sigma}{d^3C} = I(\epsilon) \epsilon^{F+1+H} (1-x_R z)^{-F-} (1+x_R z)^{-F+} J(C_T^2) , \quad (5.12)$$

where  $z = \cos \theta_{cm}$ ,  $F- = 1 + g_a$ ,  $F+ = 1 + g_b$ . As before  $F = 1 + g_a + g_b$ , and  $I(\epsilon)$  is a slowly varying function of  $\epsilon$  above any quasielastic peak. This result is valid for an inclusive internal process parametrized in the form

$$\sim (1-x'_R)^H J(C_T^2) .$$

If need be, this form can be easily generalized. Although Eq. (III-20) was derived assuming  $|z|$  not near one (outside the forward and backward cones), we see that it also has the correct limit inside those regions. This expression can

then be used to characterize inclusive nuclear reactions at all angles. Furthermore since we expect a smooth transition from the regions of validity of Eq. (5.12) to other regions of the Peyrou plot; for example, the central region, this equation can be used to fit the data everywhere with effective powers  $F, F_-, F_+$ .

## VI. PION AND PROTON YIELDS AND FORM FACTORS

As the first application of the model, consider  $\pi^-$  production in the projectile fragmentation region. The small angle data in Fig. 4 taken from J. Papp et al.,<sup>9</sup> clearly supports the value  $H=3$ . The value of  $T$  now can be determined by looking at deuteron beam data. The fit for  $T=3$  is compared with the data in Fig. 5. Now all parameters are fixed and the prediction for alpha beams is compared with the data<sup>2</sup> in Fig. 6.

The proton yield in the forward and backward direction is fully determined since it depends only on  $T$  ( $H=-1$ ). For these reactions the data is not as extensive in the variable  $x_F$  as in the pion data so the tests are not as severe. The reaction  $d+C \rightarrow p+X$  is predicted to go as  $\epsilon^5$ . The data is in reasonable agreement with this behavior but it does not fall quite this fast for the largest  $x_F$  values. The prediction for the proton yield from carbon-carbon collisions is compared with the data in Fig. 7.

It will be very interesting to extend the above discussions to other energies and reactions and to compare theory with experiment. Of particular importance here is measurements over the entire angular range to check the validity of Eq. (5.12). These will be forthcoming, I understand, from the Berkeley group. NOTE: In particular reactions, and especially at lower energies, the nuclei may not completely fragment so that a value of  $A_{\text{eff}} < A$  may have to be used to fit the data here. Thus even at low energies it may be useful to fit the form (5.12) to the data and to extract values of  $F$ ,  $F_+$ , and  $F_-$ . If they can be interpreted in terms of an  $A_{\text{eff}}$ , this interpretation can be checked by comparing with other yields (the pion to the proton for example).

Let us now discuss the nuclear form factor arising from the model wave functions that fit the inclusive data ( $T=3$ ). We are concentrating on the short

distance or large  $q^2$  behavior, and hence will make no attempt to fit diffraction etc., that arise from effects of the edge of the nucleus. The form factor is written as

$$F_A(q^2) = \sum_a F_a(q^2) \int \frac{dx d^2 k_T}{2(2\pi)^3} \frac{x}{(1-x)} \psi_a^*(x, \vec{k}_T + (1-x)\vec{q}_T) \psi_a(x, \vec{k}_T) ,$$

where the sum runs over the nucleons (protons and neutrons) in the nucleus A.  $F_a(q^2)$  has been replaced by its on-shell value, and the integral multiplying it is then the intrinsic body form factor of the nucleus.

A very plausible wave function  $\psi$  which we saw before gives a G function with many correct properties, is

$$\psi(x, \vec{k}_T) = \frac{N(x)(1-x)^{\frac{g+1}{2}}}{\left[ k_T^2 + M^2(x) \right] \left[ k_T^2 + M^2(x) + \delta^2 \right]^{\frac{g-1}{2}}}$$

where for the case of the deuteron  $g=5$  for  $T=3$  (the exchange of vector mesons with monopole form factors at each vertex).

First, since  $\psi$  describes one off-shell and one on-shell particle, neither  $\psi$  nor  $G$  are necessarily symmetric around  $x = 1/2$ . Isospin symmetry implies that  $G_{p/D}(x) = G_{n/D}(x)$ , not that  $G_{p/D}(x) = G_{n/D}(1-x)$ . However, this is a good approximation at not too high energies, when we consider a deuteron as composed of only one proton and one neutron, which means

$$\int dx d^2 k_T G_{a/D}(x, \vec{k}_T) = 1 .$$

Note that then this is equivalent to a momentum normalization condition. The symmetry of  $G$  around  $x = 1/2$  fixes the function  $N(x) = N_0 x^2$ . The deuteron form factor can now be computed. A fit that can be achieved for our spinless model is given in Fig. 8 for the value

$$\delta_D^2 \simeq 200 M \epsilon \quad ,$$

where  $M$  is the nucleon mass and  $\epsilon$  is the binding energy of the deuteron. Here the isoscalar form factor was taken to be equal to the proton form factor. This is the same  $\delta_D^2$  value that was used to fit quasielastic scattering discussed earlier. The data is from Ref. 10. If spin were put into the model, and especially if D-state effects were then included, the fit could be made much better since the quadrupole contribution naturally gives a shape that is similar to that of the data points.

Predictions have been made by I. Schmidt<sup>3</sup> for the  $\text{He}^3$  and  $\text{He}^4$  form factors out to a  $(-q^2)$  of  $6 (\text{GeV}/c)^2$ . These will soon be measured at SLAC, and will provide new tests for the model. Finally, note that  $T=3$  is the same behavior as expected by quark counting,<sup>11</sup> as was pointed out before.

## VII. STRUCTURE FUNCTIONS AND NONSCALING

Since we now have a relativistic wave function for the deuteron that fits both inelastic inclusive scattering and the elastic deuteron form factor, it can be used to describe deep inelastic electron scattering from the deuteron. A separation of the neutron and proton structure functions can then be performed with some confidence in regions where one would not trust a nonrelativistic treatment.<sup>12</sup> To discuss inelastic scattering we simply return to Fig. 1 and Eq. (2.1) and set  $B=b=C=\text{electron}$ , and consider the various choices for  $a$  and  $d$ . A classification of the terms contributing to the deuteron structure function is given in Fig. 9. In Fig. 9c, the two nucleons recoil coherently, sharing the  $q^2$  of the virtual photon. This is small for large  $q^2$ . In the second term, Fig. 9b, one has  $d=\text{nucleon}$  (or baryon resonance), and it recoils with momentum  $q$ . This term may be important for moderate  $q$  values, and is given by terms of the form ( $a = \text{proton or neutron}$ )

$$\sim x_D G_{a/D}(x_D) F_a^2(q^2) \quad , \quad (7.1)$$

where  $F_a(q^2)$  is the dipole form factor of the nucleon.

The first term Fig. 9a is inelastic scattering from the nucleon and is given in terms of their structure function  $F_{2a}(x, q^2)$  (which may not scale):

$$\sim \int_{x_D}^1 dy F_{2a}(x_D/y, q^2) G_{a/D}(y) \quad , \quad (7.2)$$

which clearly vanishes faster than (7.1) as  $x_D \rightarrow 1$ . Note that if  $G_{a/D}(y)$  is strongly peaked at  $y=1/2$ , which is certainly true in the limit of zero binding, this contribution becomes

$$\sim F_{2a}(2x_D, q^2) \theta(1-2x_D) \quad ,$$

which has a simple physical interpretation.

These contributions have been used to describe inelastic scattering from the deuteron from low to high  $q^2$  values and to extract the neutron structure function.<sup>13</sup> We will not go into this in detail but will use the physical picture described above in which coherent recoils in the final state lead to nonscaling terms that fall in  $q^2$  but vanish less rapidly as  $x \rightarrow 1$ . Examples are shown in Fig. 10 for the nucleon. Figure 10a has a single recoil quark, 10b has a recoil diquark and meson system, and 10c depicts a recoil baryon (or baryon resonance) system. The last three terms are not important in the range of large to moderate  $q^2$  and large  $x$  and will be neglected.

Using our previous rules, ( $T=1$  of course), and dimensional counting for the form factors, the diquark term is of the form

$$F_{2a}^d(x, q^2) = A_d F_d^2(q^2) x^2 (1-x) \quad (7.3)$$

where

$$F_d(q^2) = d^2 / (d^2 - q^2)$$

is the diquark form factor. The valence, or large  $x$ , part of Fig. 10a will be written in the form

$$\sim A(x)(1-x)^3 \quad ,$$

where  $A(x)$  is finite at  $x=1$  and slowly varying.

The total nucleon structure function will be written in the form

$$F_{2a}(xq^2) = A^a(x)(1-x)^3 + A_d^a F_d^2(q^2) x^2 (1-x) \quad , \quad (7.4)$$

and the main question is whether or not this will fit the data for large  $x$ , say  $x > 0.2$ , with an  $A(x)$  that does not depend on  $q^2$ . If this is possible, then we have possibly identified important contributions to nonscaling that have a very simple and expected physical origin. Note that the sea is in  $A(x)$ —that is, there is a term that vanishes as  $(1-x)^4$  that measures the amount of  $(q\bar{q})$  sea present. It is not important for  $x > 0.2$ , our region of primary interest.

Suffice it to say, the fits are very good for all  $x$  and for  $x > 0.2$ ,  $A(x)$  is independent of  $q^2$ . The final results are shown in Fig. 11 for the proton structure function. Since the deuteron was treated earlier, one may extract the neutron structure function which is shown also in Fig. 11. The diquark term is quite small, but fits all the scale breaking for  $q^2 > 2$ ,  $x > 0.2$ .

Note that the ratio of  $A(x)$  for the proton to that for the neutron is  $\approx 3/2$ , which is the ratio of the squares of the valence quark charges. Also, the ratio of the diquark term for proton/neutron is  $\approx 3$ , which is the ratio of the squares of the diquark charges! This agreement is an amusing feature of our model and show its consistency if not correctness. There are, however, other ways to fit this data, using QCD, for example, and its asymptotic freedom behavior but the particular method as applied seems questionable to me (i. e., believing in a leading log expansion and even a leading log log expansion), and the resultant mass scale (the  $\Lambda^2$  in the coupling constant) seem highly artificial. However, taste aside, this may be correct. What seems more likely to me is that each is  $\approx 1/2$  the truth.

Finally these functions can be applied<sup>12</sup> to neutrino data and fit quite well the main features of the data without any change in the parameters (for example, the lack of nonscaling seen in the new data for  $x < 0.2$ ).

Recalling the comments in Section III, we see that here too we disagree with the conventional QCD calculations for the structure functions. For example, if a virtual gluon makes a  $q\bar{q}$  pair, the  $\bar{q}$  structure function is dominated by antiquarks near their mass shell (if one does not take too seriously the leading log approximation). Thus the  $\bar{q}$  is around a long time (by the uncertainty principle), interacts with the other quarks, "thermalizes", and produces a  $(1-x)^7$  behavior in  $G_{\bar{q}/p}^8$ .

### VIII. MASSIVE LEPTON PAIRS

Before considering purely hadronic processes, let us consider an intermediate one—the production of a massive lepton pair by hadron beams (inclusive inverse "photo"-production, where the virtual photon produces the lepton pair). Let us reiterate the points made in Section III about coherence and the hard scattering expansion. The total yield is a sum over intermediate states a and b (and the final state d). These terms must be incoherent—and this requires, for example, that a beam fragment in one term (in the sum over a and b) not be allowed to end up in the same part of phase space as an identical fragment from the central process of another term in the sum (all other particles being the same). This is a difficult requirement to enforce with mathematical precision. Clearly one can easily make a mistake in this regard if large momentum transfer scattering is allowed in both the beam or target vertex (or structure) function and the central scattering process. Simply adding a broad transverse momentum to the beam fragmentation function can lead to double counting (as well as trouble with gauge invariance in the present reaction). To avoid this problem we shall insist that all large momentum transfer scatterings occur in the central process only. In this way we can avoid double counting and coherence problems but yet can include all possible diagrams.

The full cross section of a beam particle A on target particle B is found to be

$$Q^4 \frac{d\sigma}{d^4Q} (AB \rightarrow \ell^+ \ell^- X) = \sum_{a, b, d} \int dx dy G_{a/A}(x) G_{b/B}(y) Q^4 \frac{d\sigma}{d^4Q} (ab \rightarrow \ell^+ \ell^- d; s' t' u'; Q^2) \quad (8.1)$$

The easiest way to enforce gauge invariance (not the only way) is to assume that the basic process is meson-quark  $\rightarrow (\ell^+ \ell^-)$ -quark.<sup>4</sup> This model

allows the rate to be normalized in two different ways and yet in the correct physical limit, is identical to the Drell-Yan model of  $q\bar{q}$  annihilation. In Ref. 4, the cross section for meson + quark  $\rightarrow l^+ l^- +$  quark, was shown to be (see Fig. 12b)

$$Q^4 \frac{d\sigma}{d^4Q} (Mq \rightarrow l^+ l^- q) = \frac{1}{6\pi^2} \alpha^2 h^2 \delta(s+t+u-Q^2 - 2M^2) \Sigma(s, t, u; Q^2) \quad (8.2)$$

where  $\Sigma$  is a simple function given there.

We are not interested in a quantitative evaluation of the cross section but rather in qualitative behavior in different regions of phase space.

The large  $Q_T^2$  and  $Q^2$  distributions can be extracted from the above formulas by writing  $xG_{a/A}(x) \propto (1-x)^{g_a}$ , and similarly for  $b/B$ . By manipulations similar to those used to extract the large transverse momentum behavior in hard scattering models, but which are more involved because both  $Q^2$  and  $Q_T^2$  are large, it is possible to derive the form

$$Q^4 \frac{d\sigma}{d^4Q} (AB \rightarrow l^+ l^- X) \cong K(Q_T^2, Q^2) \epsilon^F J(\epsilon, x_F) \quad +8.3$$

and

$$K(Q_T^2, Q^2) = \left(1 + \frac{Q_T^2}{\mu^2}\right)^{-2} \left(1 + \frac{Q_T^2}{\mu^2 + dQ^2}\right)^{-1}, \quad (8.4)$$

where  $\mu$  is a mass parameter related to internal masses in the model,  $d$  is a constant ( $d \approx 1$ ),  $J$  is slowly varying for small  $\epsilon$ , and  $F=1+g_a+g_b$ . This is a universal characterization of the  $Q_T$  distribution for all beam particles (since  $\mu$  and  $d$  are the same). Finally

$$\epsilon = \frac{\mathcal{M}^2}{s} = 1 - \frac{t+u}{s} - \frac{Q^2}{s}, \quad (8.5)$$

where  $\mathcal{M}$  is the total missing mass with respect to the photon (hadron masses were neglected in the above kinematics). This form can be used to parametrize detailed numerical calculation and may prove useful in fitting data. After

integrating over  $Q_T^2$ , the factors  $\epsilon^F J(\epsilon, x_F)$  are simply related to the folding of structure functions in the Drell-Yan formula. The explicit  $\epsilon^F$  factor characterizes the threshold behavior. After integrating over  $x_F$  and  $Q_T^2$ , which adds an extra factor of  $\epsilon^2$ , the threshold behavior for the mass distribution  $d\sigma/dQ^2$  is  $\epsilon^{F+2}$ . For D-Y, this final power is 11 for pp scattering and 5 for  $\pi p$  scattering if one uses the dimensional counting predictions for the structure functions.<sup>8</sup> For the meson-quark scattering case,  $F=9$  and 3, respectively (again using dimensional counting), hence the final  $\epsilon$  power is the same in the two cases. This is not unexpected since the first diagram in Fig. 12b is clearly the same as the Drell-Yan mechanism. It is equally clear that the second diagram is required for gauge invariance. In fact, at large  $Q_T$ , it cancels the leading  $Q_T^{-4}$  term arising from the first diagram!

At large energies, where the  $\epsilon$  dependence can be neglected, it is easy to see that  $\langle Q_T \rangle$  has the limiting values

$$\begin{aligned} \langle Q_T \rangle &\cong \frac{\pi}{4} \mu && \mu \ll Q \\ &\cong \frac{\pi}{2} \mu (1 - 2\mu/\sqrt{s}Q) && , \quad Q \gg \mu \end{aligned} \quad (8.6)$$

a prediction that can be experimentally checked but the present data is not over a large enough range in  $Q$ . The  $\epsilon$  dependence produces an energy dependence in  $\langle Q_T \rangle$  in addition to the dependence on  $Q$ . A very rough estimate yields

$$\frac{\langle Q_{T_s} \rangle}{\langle Q_{T_{s'}} \rangle} \cong \left[ 1 + \pi \mu \left( \frac{1}{\sqrt{s'}} - \frac{1}{\sqrt{s}} \right) \right]^F, \quad (8.7)$$

which can be a growth of  $\approx 30\%$  over the ISR energy range.

### IX. HADRONS AT LARGE TRANSVERSE MOMENTUM

In order to treat hadrons, we simply consider quarks as the constituents with a normal gluon interaction (thus  $T=1$ ) and apply our previous formulas. The main difference is that it is customary to interchange A and B in our previous discussion and to consider A as the beam particle. This changes only the notation, not the physics! First a review of some relevant experimental results and numbers.

The fixed angle ( $90^\circ$  center of mass) exclusive two-body cross sections at large  $s$  will be parametrized in the form

$$\left. \frac{d\sigma}{dt} \right|_{90^\circ} = E s^{-n} \quad (9.1)$$

Throughout the paper pure GeV units will be used. Inclusive large  $p_T$  cross sections at  $90^\circ$  center of mass from FNAL<sup>1,2</sup> and the ISR<sup>3,4</sup> can be fit to the form ( $\epsilon = 1 - 2 p_T/\sqrt{s} = 1 - x_T$ )

$$E \left. \frac{d\sigma}{d^3p} \right|_{90^\circ} = I \epsilon^F \left( p_T^2 \right) \quad \begin{cases} x_T > 0.2 \\ 2 < p_T < 8 \text{ GeV}/c \end{cases} \quad (9.2)$$

Table I summarizes the values for I, N, F, and E, n for the various well-known cross sections of interest.<sup>14</sup> For N and F we have chosen the nearest integer values, and then fit the normalization constant I.

The reactions  $pp \rightarrow K^- X$  or  $\bar{p} X$  near  $90^\circ$  can be fit by the following behavior ( $\epsilon < 1$ ):

$$\frac{E \frac{d\sigma}{d^3p} (pp \rightarrow K^- X)}{E \frac{d\sigma}{d^3p} (pp \rightarrow K^+ X)} \approx 1.0 \epsilon^{3.5} \quad (9.3)$$

$$\frac{E \frac{d\sigma}{d^3p} (pp \rightarrow \bar{p} X)}{E \frac{d\sigma}{d^3p} (pp \rightarrow p X)} \approx 0.3 \epsilon^{6.9 \pm 2.4} \left( p_T^2 \right)^{1.4 \pm 1.3} \quad (9.4)$$

Table I  
(GeV Units)

Reaction	<u>E</u>	n		
$pp \rightarrow pp$	$1.2 \times 10^9$	10		
$\pi^\pm p \rightarrow \pi^\pm p$	$2.5 \times 10^4$	8		
$\pi^- p \rightarrow \pi^0 n$	$2.5 \times 10^4$	8		
$\gamma p \rightarrow \pi^+ n$	$1.2 \times 10^1$	7		
<u>Reaction</u>	<u>I</u>	<u>N</u>	<u>F</u>	
$pp \rightarrow \pi^{+,0,-} X$	(9, 8, 7)	4	9	
$pp \rightarrow K^+ X$	5	4	9	
$pp \rightarrow p X$	500	6	7	
$\pi^\pm p \rightarrow \pi^0 X$	3.5	4	7	

By analyzing data on the momentum distribution of particles balancing a large  $p_T$  trigger, one can estimate that between 1/2 and 1/4 of the trigger particles are "prompt" as opposed to those that arise from the decay of produced resonances. We shall attempt to compute the yield of the prompt component only, which we take to be roughly 1/3 of the values of I given in Table I.

An example of the quality of the fit is shown in Fig. 13 taken from Cronin et al., Ref. 14.

We first need to choose simple forms for the G functions in order to compute the yields<sup>15</sup>. The G's are constrained to satisfy the spectator counting rules<sup>6</sup> as  $x \rightarrow 1$  (with T-1) and to have a reasonable shape for small x (i. e., some flattening off in xG). A form (Fig. 14) with these properties which yields simple integrals in later calculations is

$$\begin{aligned}
 xG_{a/A}(x) &= (1 + g_a) f_{a/A} N(a/A) (1-x)^{g_a} & x > \hat{x}_a \\
 &= (1 + g_a) f_{a/A} N(a/A) (1-\hat{x}_a)^{g_a} & x < \hat{x}_a,
 \end{aligned}
 \tag{9.5}$$

where

$$g_a = 2n(\bar{a}A) - 1$$

and  $n(\bar{a}A)$  is the minimum number of quarks in the spectator system. Here

$f_{a/A}$  is the fraction of total momentum carried by a in A

$$f_{a/A} \equiv \int_0^1 dx xG_{a/A}(x) \tag{9.6}$$

and

$$N(a/A) = \left[ (1-\hat{x}_a)^{g_a} (1 + g_a \hat{x}_a) \right]^{-1} \tag{9.7}$$

As an example, reasonable values for u or d quarks in a proton are  $g_a=3$  and  $\hat{x}_a = 0.25$ .  $N(a/A)$  adjusts for the shape dependence of the structure function relative to a pure  $(1-x)$  power and approaches 1 as  $\hat{x}_a \rightarrow 0$ . Throughout these lectures if "a" refers to a quark, it will be a quark of a given color. This means that there will be many odd looking factors of 3 in our formulas that are due to color sums and normalizations.

In order to assign values to the momentum fractions  $f$  (of mesons in a proton, for example), it is necessary to use the convolution formula

$$G_{a/A}(x) = \sum'_n \int_x^1 \frac{dz}{z} G_{a/n}^V\left(\frac{x}{z}\right) G_{n/A}(z) \tag{9.8}$$

Note that to avoid double counting one of the  $G$ 's must be "irreducible," i.e., a valence distribution function, and the sum,  $\sum'$ , is restricted to non-overlapping intermediate particle states ( $n$ ) having no quarks in common. A simple integration yields

$$f_{a/A} = \sum_n^V f_{a/n}^V f_{n/a} \quad (9.9)$$

Using the above formulas and experimental data wherever possible, such as for the quark and antiquark distributions, one arrives at the values given in Table II. These will be used in our later calculations of note.

In a scale invariant theory all exclusive differential cross sections at large momentum transfers in the fixed angle regime can be written as a sum of terms of the form

$$\frac{d\sigma}{dt} = \pi \mathcal{D} s^{T+U-N} (-t)^{-T} (-u)^{-U} \quad (9.10)$$

where  $\mathcal{D}$  contains the relevant coupling constants. This parametrization is appropriate for general processes involving quarks, gluons and hadrons.

There are two critical coupling constants for quark-hadron scattering which we now define. For the coupling of a meson to its simplest valence two-quark component, we define a standard coupling,  $g/\sqrt{3}$ , of the  $\pi^+$  to a  $u$  and  $\bar{d}$  quark of one color. We also define  $h/\sqrt{3}$  to be the coupling of a quark of one color to a baryon. Defining standard values

$$\alpha_M = \left( \frac{1}{3} \frac{g^2}{4\pi} \right) \quad \alpha_B = \left( \frac{1}{3} \frac{h^2}{4\pi} \right) \quad (9.11)$$

we give in Table III the cross section forms for all elementary processes of interest for quarks interacting with  $J^P = 0^-$  mesons and  $J^P = \frac{1}{2}^-$  baryons. One should take special note that the  $\gamma q \rightarrow Mq$  cross form given in the table incorporates three additional diagrams, other than the one drawn, as required by gauge invariance. All cross sections are those for quarks or diquark systems of one given color. The spin 1/2 quark spin 1 vector gluon structure of QCD is reflected in the tabulated results. For instance the  $qM \rightarrow qM$  cross section in a scalar quark  $\phi^4$  model is proportional to  $1/s^2 u^2$  instead of  $1/su^3$  as found for spin 1/2 quarks. The latter value is in the table.

Table II

Distribution Function Parameters (per color)

$$xG_{a/A}(x) = (1 + g_a) f_{a/A} N(a/A) (1-x)^{g_a} (x > \hat{x}_a)$$

a/A	$g_a$	$\hat{x}_a$	$f_{a/A}$	N(a/A)
u/p	3	.2	.1	1.22
d/p	3	.2	.067	1.22
$\bar{q}/p$	7	0	.01	1
(2q)/p	1	.6	.1	1.6
M/P	5	.3	.1	2.4
$K^-/P$	9	0	.024	1
B/P	3	.5	.12	3.2
q/ $\pi$	1	.3	.083	1.1
$\bar{q}/\pi$	1	.3	.083	1.1
M/ $\pi$	3	.4	.1	2.1

$$f_{u/p}^V = 2 f_{d/p}^V = .04$$

$$f_{q/M}^V = f_{\bar{q}/M}^V = .033$$

$$\sum_M f_{M/p} = .1$$

$$\sum_B f_{B/p} = .18$$

$$\sum_M f_{M/p} \cong .4$$

$$\sum_B f_{B/p} \cong .72$$

$$\sum_M f_{M/\pi} \cong .8$$

$$\sum_{q=u, V} f_{q/p} = .17$$

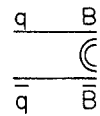
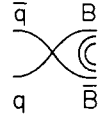
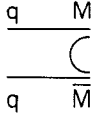
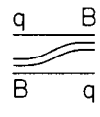
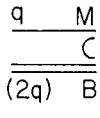
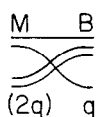
$$\sum_{\bar{q}} f_{\bar{q}/p} = .03$$

$$\sum_q f_{q/\pi} = \sum_{\bar{q}} f_{\bar{q}/\pi} = .083$$

$$\sum_{(2q)} f_{(2q)/p} = .3$$

TABLE III  
ELEMENTARY CIM SUB PROCESSES (Spin and Color Averaged)

$$\frac{d\sigma}{dt} = \frac{\pi\mathcal{D}}{s^2} \times \overline{\sum \mathcal{M}^2}$$

Subprocess	$\mathcal{D}$	$\overline{\sum \mathcal{M}^2}$	Subprocess	$\mathcal{D}$	$\overline{\sum \mathcal{M}^2}$
$qM \rightarrow qM$ (ut) 	$\alpha_M^2$	$\frac{s}{u^3}$	$d\bar{d} \rightarrow p\bar{p}$ 	$\alpha_B^2$	$\frac{s^2+u^2}{s^2t^4}$
$qM \rightarrow qM$ (st) 	$\alpha_M^2$	$\frac{u}{s^3}$	$\bar{d}d \rightarrow p\bar{p}$ 	$\alpha_B^2$	$\frac{s^2+t^2}{s^2u^4}$
$q\bar{q} \rightarrow M\bar{M}$ 	$\frac{1}{2}\alpha_M^2$	$\frac{u}{t^3}$	$\bar{d}p \rightarrow p\bar{d}$ 	$\alpha_B^2$	$\frac{t^2+u^2}{u^2s^4}$
$Mq \rightarrow \gamma q'$ (ut) 	$2\alpha\alpha_M$	$\frac{1}{s^2t}(s^2+u^2)\left(\frac{\lambda\bar{q}}{u} - \frac{\lambda q'}{s}\right)^2$	$dp \rightarrow pd$ 	$\alpha_B^2$	$\frac{s^2+u^2}{u^2t^4}$
$\gamma q \rightarrow Mq'$ (ut) 	$\alpha\alpha_M$	$\frac{1}{s^2t}(s^2+u^2)\left(\frac{\lambda\bar{q}'}{u} - \frac{\lambda q}{s}\right)^2$	$q(2q) \rightarrow MB$ 	$\frac{1}{2}\alpha_B\alpha_M$	$\frac{u}{t^5}$
$dp \rightarrow dp$ (ut) 	$\alpha_B^2$	$\frac{s^2+t^2}{t^2u^4}$	$(2q)M \rightarrow Bq$ 	$\alpha_B\alpha_M$	$\frac{s}{u^5}$

The exclusive scattering process  $AB \rightarrow CD$  (see Fig. 3a) can be considered as the scattering of  $A \rightarrow C$  off of a quark constituent of the target B. Since the constituent in general has some fraction,  $x$ , of the target momentum, the basic subprocess occurs at a reduced energy and one readily shows from this quark interchange diagram that

$$\frac{d\sigma}{dt} (AB \rightarrow CD) = F_{BD}^2(t) N_{\text{coh}}^2 \frac{d\hat{\sigma}}{dt} (Aq \rightarrow Cq; s = \langle x \rangle s, t = t, u = \langle x \rangle u) + \text{permutations } (A, C \rightarrow B, D) \quad , \quad (9.12)$$

where the form factor reflects the sticking probability in the final state and the mean value theorem has been used to replace  $x$  under the integral by  $\langle x \rangle$ ,

$N_{\text{coh}}$  is the number of coherently interfering diagrams which contribute. Using the standard form for  $d\hat{\sigma}/dt$ , Eq. (9.10), defining  $n=4+N$ , and taking

$F_B(t) = \left(1-t/M_V^2\right)^{-2}$  for a proton target, we obtain at large  $s$

$$s^n \frac{d\sigma}{dt} \Big|_{90^\circ} = E_{e\ell} (AB \rightarrow CD) = \pi \langle x \rangle^{T-N} N_{\text{coh}}^2 2^{4+T+U} (M_V)^8 \quad , \quad (9.13)$$

which is consistent with dimensional counting. One expects that  $\langle x \rangle \gtrsim 1/3$  should characterize scattering from a valence component of the proton target.

Using the above formula, and the values of  $T$  and  $U$  from Table III, one finds by fitting the data for  $E$  that

$$\alpha_M = 1.2 \text{ GeV}^2, \quad \alpha_B = 10 \text{ GeV}^4 \quad (9.14)$$

which we adopt as standard values. These values also give reasonable numbers when one computes momentum fractions such as  $f_{\bar{q}/M}$  and  $f_{q/p}$ . This consistency further supports the model.<sup>15</sup>

It is apparent that the direct inclusive process,  $AB \rightarrow CX$ , in which the beam does not radiate prior to interacting with a constituent of the target, is obtained

from the previously quoted exclusive scattering formula by replacing the form factor by the relevant target structure function. A simple calculation then leads to the result

$$E_c \frac{d\sigma}{d^3 p_c} (AB \rightarrow CX) = \frac{1}{\pi} \frac{s}{s+u} 3 \sum_{b,d} x G_{b/B}(x) \cdot \frac{d\hat{\sigma}}{dt} (Ab \rightarrow Cd', s' = xs, t' = t, u' = xu) \quad (9.15)$$

The sum of  $b, d$  is over quark flavors and the explicit 3 results from the sum over colors. The structure function  $G$  and  $d\sigma/dt$  are for quarks of one given color. The variables used to describe inclusive scattering subprocess cross section  $A + B \rightarrow C + X$  are

$$s + t + u = \mathcal{M}^2 = \epsilon s,$$

where  $\mathcal{M}$  is the total missing mass and

$$\begin{aligned} x_1 &= -u/s = \frac{1}{2} x_R (1 + z) \\ x_2 &= -t/s = \frac{1}{2} x_R (1 - z) \end{aligned} \quad (9.16)$$

where

$$\epsilon = 1 - x_R, \quad x_R \cong E^{\text{cm}}/E_{\text{max}}^{\text{cm}},$$

and  $z (= \cos \theta)$  is the cosine of the center-of-mass scattering angle. The on-mass-shell condition for particle C determines  $x$  in Eq. (9.15) to be

$$x = x_2/(1-x_1) \quad .$$

For  $x > \hat{x}_b$  one may substitute the simple forms for  $G_{b/B}$  and  $d\sigma/dt$  from (3.1) and (3.6) and obtain

$$E_c \frac{d\sigma}{d^3 p_c} = 3 \mathcal{D} \sum_{b,d} (1+g_b) f_{b/B}^{N(b/B)} x_1^{N-U} (1-x_1)^{N-T-1-g_b} K(g_b, N) \quad (9.17)$$

where the dominant dynamical variation in  $\epsilon$  and  $p_T$  is contained in

$$K(F, N) = \epsilon^F (p_T^2 + M^2)^{-N} , \quad (9.18)$$

and the effective mass scale  $M$  is less than  $\sim 1$  GeV.

The double bremsstrahlung process depicted in Fig. 1 is easily evaluated using the  $G$  functions and  $d\sigma/dt$  forms already discussed. The result can be written in the form

$$E_C \frac{d\sigma}{d^3 p_C} = 3 \sum_{a,b} I(a,b) K(F, N; F^+, F^-) J(\epsilon, z) . \quad (9.19)$$

Here we have employed (as appropriate for all our CIM applications) the presence of one quark-loop color sum. The sum is over the flavors of the interacting constituents, and

$$I(a,b) = \mathcal{D} f_{a/A} f_{b/B} N(a/A) N(b/B) 2^{F^+ + F^-} \frac{\Gamma(2 + g_a) \Gamma(2 + g_b)}{\Gamma(2 + g_a + g_b)} . \quad (9.20)$$

The main dynamical behavior is contained in the  $K$  function

$$K(F, N; F^+, F^-) \equiv \epsilon^F (p_T^2 + M^2)^{-N} (1 + x_R z)^{-F^+} (1 - x_R z)^{-F^-} \quad (9.21)$$

Note that the effective power of  $\epsilon = (1 - x_R)$  changes as one approaches  $z = \pm 1$ .

Also note the similarity to formula (5.12) which we derived in the nuclear case.

The parameters in the above are given by

$$\begin{aligned} F &= 1 + g_a + g_b \\ F^+ &= 1 + U + g_a - N \end{aligned} \quad (9.22)$$

and

$$F^- = 1 + T + g_b - N ,$$

all of which can be easily calculated by quark counting and reference to Table III for  $T$  and  $U$  values.

For generality let us write the structure functions in a slightly more general form than Eq. (9.5), namely

$$xG_a(x) = f_a N_a (1+g_a)(1-x)^{g_a} R_a(x) \quad (9.23)$$

where, as in our (9.5) example,  $R_a(x) = 1$  for  $x > \hat{x}_a$ , and  $R_a(x) = ((1-\hat{x})/(1-x))^{g_a}$  for  $x < \hat{x}$ . Using this form, the slowly varying factor J becomes

$$J(\epsilon, z) \equiv \frac{\Gamma(2+g_a+g_b)2^{-F}}{\Gamma(1+g_a)\Gamma(1+g_b)} \int_0^1 d\eta (1+\eta)^{g_a} (1-\eta)^{g_b} H(\eta) \quad , \quad (9.24)$$

where

$$H(\eta) = \left[ \frac{1+z x_R}{1+z x_R + \epsilon \eta} \right]^{F^+} \left[ \frac{1-z x_R}{1-z x_R - \epsilon \eta} \right]^{F^-} \cdot R_a \left( \frac{x_R(1+z)}{1+z x_R + \epsilon \eta} \right) R_b \left( \frac{x_R(1-z)}{1-z x_R - \epsilon \eta} \right) .$$

One can see that for  $x_R > \frac{1}{2}(\hat{x}_a + \hat{x}_b)$ , and for z not too near  $\pm 1$ ,  $J(\epsilon, z) \approx 1$ . We have found that for the relevant values of  $g_a$ , etc., J can differ from one by typically 20 or 30% in the interesting experimental range, say  $\epsilon < 0.7$ .

Setting J=1 allows us to make simple predictions for the prompt rate of production of mesons, baryons, antibaryons, etc. All constants are now known.

For meson production from a proton beam, we will write down the complete answer (the only time I dare!). Now the leading subprocesses which contribute to large  $p_T$  inclusive reactions are those which have the minimum  $p_T$  and  $\epsilon \rightarrow 0$  fall-off and the largest overall normalization. In this case the dominant contributions based on quark-hadron interactions arise from quark-meson scattering ( $qM^* \rightarrow qM$ ) and the fusion process ( $q\bar{q} \rightarrow M\bar{M}^*$ ). The contributions from the ut diagram Fig. 15a, and fusion diagram Fig. 15b yield

$$\begin{aligned}
 E \frac{d\sigma}{d^3p} (pp \rightarrow MX) &= \alpha_M^2 \sum_{M^*q} f_{M^*/p} f_{q/p} N(M^*/p) N(q/p) 2^6 \frac{\Gamma(7)\Gamma(5)}{\Gamma(10)} K_s(9, 4; 5, 0) \\
 &+ \frac{3}{2} \alpha_M^2 \sum_{q, \bar{q} \in M, \bar{M}^*} f_{\bar{q}/p} f_{q/p} N(\bar{q}/p) N(q/p) 2^7 \frac{\Gamma(9)\Gamma(5)}{\Gamma(12)} K_s(11, 4; 7, -1) \\
 &+ \frac{3}{2} \alpha_M^2 \sum_{\bar{q}, q \in M, \bar{M}^*} f_{\bar{q}/p} f_{q/p} N(\bar{q}/p) N(q/p) 2^7 \frac{\Gamma(9)\Gamma(5)}{\Gamma(12)} K_s(11, 4; 3, 3),
 \end{aligned}$$

where  $K_s = \frac{1}{2}(K(;F^+F^-) + K(;F^-, F^+))$ . Using the numbers in the tables, the yield at  $90^\circ$ , for prompt  $\pi^+$ , from the  $qM \rightarrow qM$  plus fusion graph is

$$E \frac{d\sigma}{d^3p} (pp \rightarrow \pi^+ x) = K(9, 4) \left[ 2.2 + 0.06n(\bar{M}^*) \epsilon^2 \right] \quad (9.26)$$

where  $n(\bar{M}^*)$  is the number of states in the  $\bar{M}^*$  sum ( $\sim 3$  to  $4$ ). This equation includes the contribution from the st topology diagram of Fig. 15c which has the angular distribution  $K_s(9, 4; 1, 0)$ ; at  $90^\circ$  it contributes only  $1/4$  of that of the dominant ut contribution. Using a factor of 3 to account for the total/prompt effect, the experimental rate is roughly  $9K(9, 4)$ , compared to the prediction of  $6.6 K(9, 4)$ .

The rate for  $\pi^-$  production is somewhat smaller than for  $\pi^+$  since  $G_{u/p}/G_{d/p}$  increases as  $x$  increases. The  $\pi^+$  and  $\pi^-$  rates must be equal, however, at  $x_T = 0$ , in the Feynman scaling limit, so the  $\pi^+/\pi^-$  ratio must decrease as  $x_T$  decreases to zero. As  $x_T$  increases, however, it should rise and saturate to a constant value in the symmetric quark model used here.

The dominant  $K^-$  cross section for  $\epsilon \rightarrow 0$  arises from the fusion term. However, for moderate  $\epsilon$  it is vital to retain various contributions with higher  $\epsilon$  powers, for example  $\epsilon^{13}$ , arising from the ut and st topology  $qK^- \rightarrow qK^-$  graphs. Combining all these terms, see Fig. 15, our estimate for the  $K^-/K^*$  ratio is

$$\frac{d\sigma(pp \rightarrow K^-)}{d\sigma(pp \rightarrow K^+)} = 0.1 \epsilon^2 \frac{1+4 \epsilon^2}{1+0.07 \epsilon^2} \simeq 0.1 \epsilon^2 (1+4 \epsilon^2) \quad (9.27)$$

Recall that the numerical approximations used are not valid for  $\epsilon \rightarrow 1$  ( $x_T \rightarrow 0$ ). Experimentally, this ratio has the same shape as the above prediction but with about twice the magnitude. The fusion term dominates only for  $x_T > 0.6$ . The agreement of the model is quite good.

It is also possible to do estimates for other baryon beams. One very interesting example is

$$\begin{aligned} \frac{d\sigma(\bar{p}p \rightarrow \pi x)}{d\sigma(pp \rightarrow \pi x)} &= \frac{1+0.03 n(\bar{M}^*) \epsilon^{-2}}{1+0.03 n(\bar{M}^*) \epsilon^2} \\ &\cong 1+0.12 (\epsilon^{-2} - \epsilon^2) \quad , \end{aligned} \quad (9.28)$$

using  $n(\bar{M}^*) = 4$ . For example, at  $x_T = 0.3$ , the ratio is predicted to be 1.20.

In quark scattering models, it should be unity, thus there is not much difference until  $x_T$  is large. In a model with fusion only, the ratio would be  $\epsilon^{-4}$ , which is 4 at  $x_T = 0.3$ .

We haven't time to go through all possible estimates of yields, however a sampling of possible tests of our model include (these are prompt yields—multiply by 3 for total rates—see also Fig. 17):

$$E \frac{d\sigma}{d^3p} (pp \rightarrow px) = 120 x_T^2 K(3,6) \\ + 130 K(7,6) + 1.4 n(\bar{B}^*) K(11,6) ,$$

$$E \frac{d\sigma}{d^3p} (pp \rightarrow \bar{p}x) = 5.6 K(11,6) ,$$

$$\frac{d\sigma(pp \rightarrow \gamma)}{d\sigma(pp \rightarrow \pi^0)} \cong \frac{2}{3} \frac{5\alpha}{3\alpha_M} (p_T^2 + M^2) \sim 0.007 (p_T^2 + M^2)$$

$$\frac{d\sigma \pi^+ p \rightarrow \pi^0}{d\sigma(pp \rightarrow \pi^0)} = \epsilon^{-2} \frac{3}{4} \frac{\sum_q \left[ (f_{q/\pi} + f_{q/\pi}^-) N(q/\pi) + \frac{2}{5} f_{q/p} N(q/p) \right]}{\sum_q f_{q/p} N(q/p)} \\ \cong 1.0 \epsilon^{-2} .$$

$$E \frac{d\sigma}{d^3p} (\pi^+ p \rightarrow \pi^0 X) = K(7,4) \left[ 1.6 + 0.016 n(\bar{M}^*) \epsilon^{-2} + 0.35 x_T \epsilon^{-4} \right] .$$

and

$$\frac{d\sigma(\pi p \rightarrow \pi)}{d\sigma(\pi p \rightarrow p)} = \frac{\alpha_M^2}{\alpha_B^2} \epsilon^2 (p_T^2 + M^2) \frac{2^6 \cdot 5}{7} \frac{\sum_M f_{M/p} N(M/p)}{\sum_B f_{B/p} N(B/p)} \\ \sim 0.27 \epsilon^2 (p_T^2 + M^2) .$$

## X. QUARK-QUARK SCATTERING

What about quark-quark (as well as quark-gluon and gluon-gluon) scattering?<sup>16, 17, 18</sup> The relevant diagrams are shown in Fig. 18 and are easily calculated. However, in order to compute the cross section for the production of a specific hadron  $h$  one must incorporate the final state fragmentation function  $D_{h/q}$  of the quark

$$E \frac{d\sigma}{d^3p} (p_1 p_2 \rightarrow h x) = \sum_q \int_{xR}^1 \frac{dz}{2} D_{h/q}(z) E \frac{d\hat{\sigma}}{d^3p} (p_1 p_2 \rightarrow q; s, t/z, u/z). \quad (10.1)$$

Using

$$D = d \frac{(1-z)^f}{z} \quad \text{and} \quad E \frac{d\hat{\sigma}}{d^3p} = I K(F, N) \quad ,$$

one finds

$$E \frac{d\sigma}{d^3p} (pp \rightarrow h) = \sum_q d I K(F+f+1, N) \hat{J}(x_T) \quad , \quad (10.2)$$

where  $\hat{J}$  is essentially constant,

$$\hat{J} \simeq \Gamma(1+f)\Gamma(1+F) / \Gamma(2+f+F) \quad .$$

For the  $\pi^+$  yields, a reasonable fit to the quark fragmentation functions gives  $D_{\pi^+/u}$  (or  $\bar{d}$ )  $(z) = 1.0 (1-z)/z$ . Eq. (9.8) then gives at  $90^\circ$

$$E \frac{d\sigma}{d^3p} (pp \rightarrow q \rightarrow \pi^+) = K(9, 2) \alpha_s^2(0.035) \quad .$$

where we evaluated  $J(x_T)$  at  $x_T = 0.3$ . The total yield can be succinctly written in the form (adding in Eq. (9.26))

$$E \frac{d\sigma}{d^3p} = A \left[ \left( \frac{10}{p_T} \right)^8 + \left( \frac{\alpha_s}{0.15} \right)^2 \left( \frac{10}{p_T} \right)^4 \right] \epsilon^9 \quad , \quad (10.3)$$

which may prove convenient in fitting the large  $p_T$  data. Thus for  $\alpha_s = 0.15$ , the CIM diagrams dominate for  $p_T < 10$ , and one has a  $p_T^{-8}$  behavior, whereas for  $p_T > 10$ , the cross section should show a  $p_T^{-4}$  behavior. Actually, quark-gluon scattering is also important and should be added to the above estimate. Roughly speaking it doubles the second term (at least!).

## XI. FINAL REMARKS

In conclusions, I think we have shown that there is a simple model for the scattering of composite systems that works well for nucleus-nucleus scattering and for hadronic reactions. In the former case, we have been able to extend the descriptions of nuclei away from the usual and familiar nonrelativistic limit in a remarkably simple way. This application allows us to check as well the physical interpretations that we make in the considerably more complex nuclear case.

In the hadron case, I would argue that the CIM diagrams must be included in any complete treatment and to omit them would be internally inconsistent. They are important because up till now, experiments are not at sufficiently large values of  $p_T$ , and their couplings ( $\alpha_M$  and  $\alpha_B$ ) are large (compared to  $\alpha_S$ ). In this regard, it is useful to distinguish three regions in transverse momentum for hadronic inclusive reactions:

(1) The asymptotically scale-free, large  $p_T$  region (above  $p_T \sim 7$  GeV for single particles, and  $p_T \sim 5$  GeV for jets), where the simple perturbation theory contributions for QCD are expected to dominate if  $\alpha_S \cong 0.3$ . In this region, strong interactions take their most elementary form,

(2) The intermediate  $p_T$  zone, where the CIM diagrams are predicted to dominate giving scaling law contributions of the form  $p_T^{-8}$ ,  $p_T^{-12}$  ... at fixed  $x_T$ , depending on the detected particle. In this region (roughly  $2 < p_T < 7$  GeV for single particle reactions), one can trace the quantum number flow characteristic of duality diagrams. In the case of exclusive reactions, Regge behavior takes its most basic form, with trajectories  $\alpha(t)$  receding to negative integers (or half-integers), or in the case of Compton scattering to a  $J=0$  fixed pole.

(3) The most complicated region is at low  $p_T$  where the cross sections Feynman-scale and many different coherent, diffractive, Regge, and resonance/cluster phenomena operate.

In the general CIM approach several different areas of hadron phenomenology become interconnected: (a) form factors, (b) large  $t$  and  $u$  exclusive reactions (c) Regge behavior at large  $t$ , (d) particle yields for  $x_L$  near  $\pm 1$  at low  $t$ , and (e) large  $p_T$  inclusive reactions. We have shown here that the normalization of the various CIM contributions to inclusive scattering are fixed by external constraints and are not arbitrary. They are of a reasonable size to explain the moderate transverse momentum single particle yields.

A theory of short distance hadronic processes patterned after asymptotically free QCD is in reasonable agreement with data, however CIM processes based on quark-hadron scattering are required for theoretical completeness and to describe the experimental data at intermediate  $p_T$ .

#### ACKNOWLEDGEMENTS

I wish to acknowledge my collaborators, I. A. Schmidt, S. J. Brodsky, M. Duong-van, and J. F. Gunion, without whom this work would not have been done. I wish to thank Dr. W. Dittrich for the kind hospitality and stimulating intellectual environment of this meeting.

REFERENCES

1. R. Blankenbecler, S. J. Brodsky, and J. F. Gunion, Phys. Lett. B39, 649 (1972); 42, 461 (1973); Phys. Rev. D12, 3469 (1975). Spectator counting rules for structure functions are derived in R. Blankenbecler and S. J. Brodsky, Phys. Rev. D10, 2973 (1974); J. Gunion, *ibid.* 10, 242 (1974). The fusion reactions  $q\bar{q} \rightarrow M\bar{M}$  have been particularly emphasized by P. V. Landshoff and J. C. Polkinghorne, Phys. Rev. D10, 891 (1974). See also M. K. Chase and W. J. Stirling, Cambridge U. preprint, DAMTP-77/15 and references therein.
2. For a general review, see D. Sivers, S. J. Brodsky, R. Blankenbecler, Physics Reports 23C, No. 1 (1976). See also Refs. 13, 15, and S. J. Brodsky, R. Blankenbecler, J. F. Gunion, XII Rencontre de Moriond, Flaine, France, March 1977.
3. I. A. Schmidt and R. Blankenbecler, Phys. Rev. D15, 3321 (1977). I. A. Schmidt, SLAC Report No. 203, 1977.
4. M. Duong-Van, K. V. Vasavada, and R. Blankenbecler SLAC-PUB-1882, Phys. Rev. D16, 1389 (1977), and M. Duong-Van and R. Blankenbecler, SLAC-PUB-2017 (Phys. Rev., in print).
5. S. D. Drell and T. M. Yan, Phys. Rev. Lett. 25, 316 (1970); Ann. Phys. 6b, 578 (1971).
6. R. D. Amado and R. M. Woloshyn, IAS preprint 77-0374 (1977). To be published in Phys. Rev.
7. There is some confusion in the literature on this point. Counting rules giving the energy dependence at fixed angle for exclusive scattering were derived by S. J. Brodsky and G. Farrar, Phys. Rev. Lett. 31, 1153 (1973); Phys. Rev. D11, 1309 (1975). V. Matveev, R. Muradyan, and A. Tavheliidze, Nuovo Cimento Lett. 7, 719 (1973).

8. Spectator counting rules giving the behavior of general G functions were first derived by R. Blankenbecler and S. J. Brodsky, Phys. Rev. D16, 2973 (1974).
9. J. Papp et al., Phys. Rev. Lett. 34, 601 (1975). J. Papp, Ph.D. Thesis, University of California, Berkeley, Report LBL-3633 (1975).
10. R. G. Arnold et al., Phys. Rev. Lett. 35, 776 (1975). Lower energy data is taken from: J. Elias et al., Phys. Rev. 177, 2075 (1969); and S. Galster et al., Nucl. Phys. B32, 221 (1971).
11. S. J. Brodsky and B. T. Chertok, Phys. Rev. D14, 3003 (1976).
12. I. A. Schmidt and R. Blankenbecler, Phys. Rev. D16, 1318 (1977). See also A. Fernandez-Pacheco, J. A. Grifols and I. A. Schmidt, SLAC-PUB-1993, (1977).
13. Compare, for example, with W. B. Atwood and G. B. West, Phys. Rev. D7, 773 (1973).
14. The data are from, for example, J. W. Cronin et al., Phys. Rev. D11, 3105 (1975). D. Antveasyan et al., Phys. Rev. Lett. 38, 112 (1977); G. Donaldson et al., Phys. Rev. Lett. 36, 1110 (1976); F. W. Busser et al., Nucl. Phys. B106, 1 (1976); and B. Alper et al., Nucl. Phys. B100, 237 (1975). See ref. 2 for a review of elastic data, and A. Eide et al., Nucl. Phys. B60, 173 (1973). See also H. I. Miettinen, SLAC-PUB-1813, presented at the Third European Symposium on Anti-nucleon-Nucleon Reactions, Stockholm (1976); J. L. Stone et al., Phys. Rev. Lett. 38, 1315, 1317 (1977); V. Chabaud et al., Phys. Lett. 41B, 209 (1972); A. Donnachie and P. R. Thomas, Nuovo Cimento 19A, 279 (1974).
15. Our discussion here follows work reported in ref. 2 and in R. Blankenbecler S. J. Brodsky and J. F. Gunion, SLAC-PUB-(to be published). For comparison see B. Pire, Phys. Rev. D15, 3475 (1977).

16. S. M. Berman and M. Jacob, Phys. Rev. Lett. 25, 1683 (1970); S. M. Berman, J. D. Bjorken, and J. B. Kogut, Phys. Rev. D4, 3388 (1971); J. Bjorken, Phys. Rev. D8, 3098 (1973). See also R. F. Cahalan, K. A. Geer, J. Kogut, and L. Susskind, Phys. Rev. D11, 1199 (1975); M. Bander, M. Barnett, D. Silverman, Phys. Lett. 48B, 243 (1974).
17. In particular see D. Sivers and R. Cutler, Phys. Rev. D16, 679 (1977) and B. Combridge, J. Kripfganz, and J. Ranft, Phys. Lett. 70B, 234 (1977).
18. In contrast see R. D. Field and R. P. Feynman, Phys. Rev. D15, 2590 (1977); R. D. Field, R. P. Feynman, and G. C. Fox, CALT-68-595 (1977); G. C. Fox, CALT-68-573 (1977).

FIGURE CAPTIONS

1. The basic hard scattering model diagram with the notation used in the text.
2. Two coherent contributions to the Drell-Yan process.
3. The wave function diagram used to compute the probability functions.
4. The  $x_F$  spectrum compared to the carbon data illustrating scaling and the value of  $H$ .
5. The prediction for  $T=3$  compared to the data of Ref. 9 for a deuteron beam.
6. The prediction for  $T=3$  compared to the data of Ref. 9 for an alpha particle beam.
7. Two inclusive processes for a carbon beam illustrating the counting rules and the positions of the quasielastic peaks.
8. Fit to the (deuteron form factor)<sup>2</sup> data of Ref. 10.
9. Contributions to the deuteron structure function, with partons of one of the nucleons (a), one nucleon (b), and both nucleons (c) recoiling coherently.
10. Contributions to the nucleon structure function, with one (a), two (b), and three (c) quarks recoiling coherently.
11. The contributions (valence, diquark and sea) and the total structure functions of proton and neutron (for  $q^2 = -5 \text{ (GeV)}^2$ ).
12. Massive lepton pair production.
13. Fit to data given by Cronin, et al., Ref. 14.
14. Simple model for  $G$ 's and their more realistic  $G$  functions.
15. Diagrams contributing to inclusive meson production.
16. Dominant contributions to  $K^-$  production.
17. Important graphs for  $B$  and  $\bar{B}$  production.
18. Quark-quark scattering diagrams.

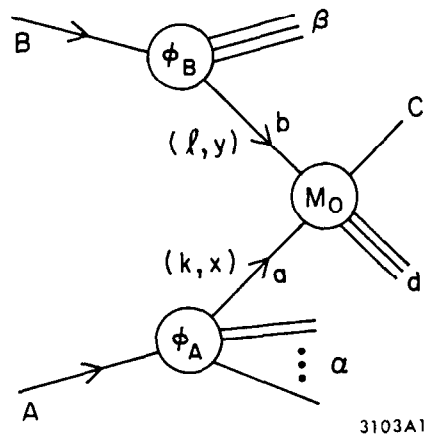


Fig. 1

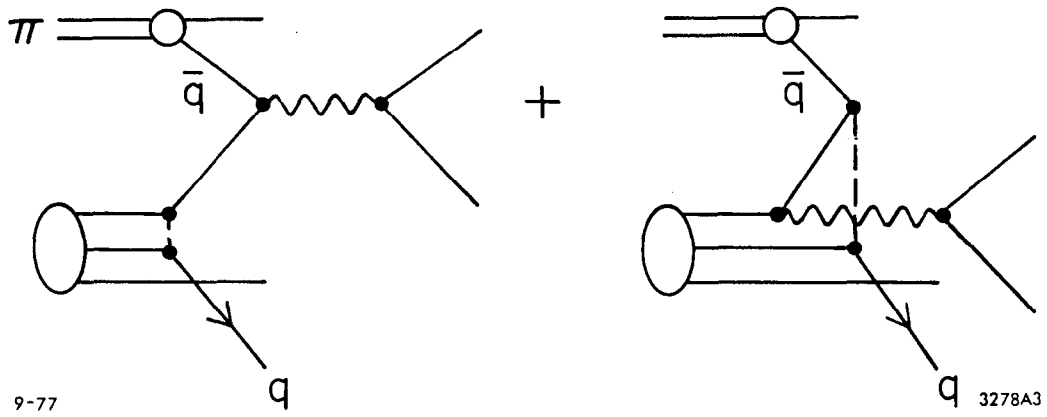
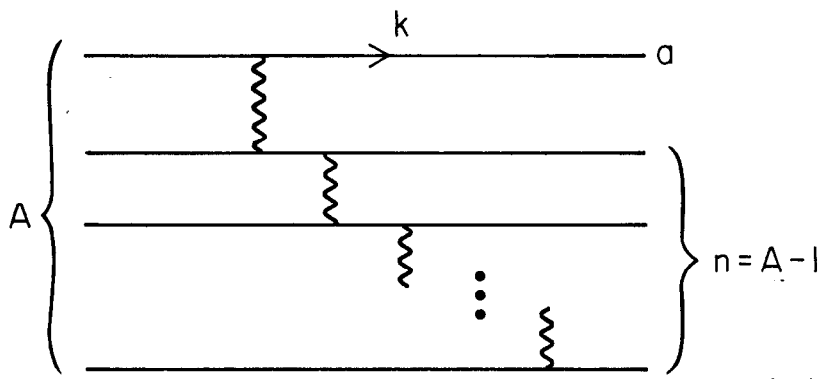


Fig. 2



3103A2

Fig. 3

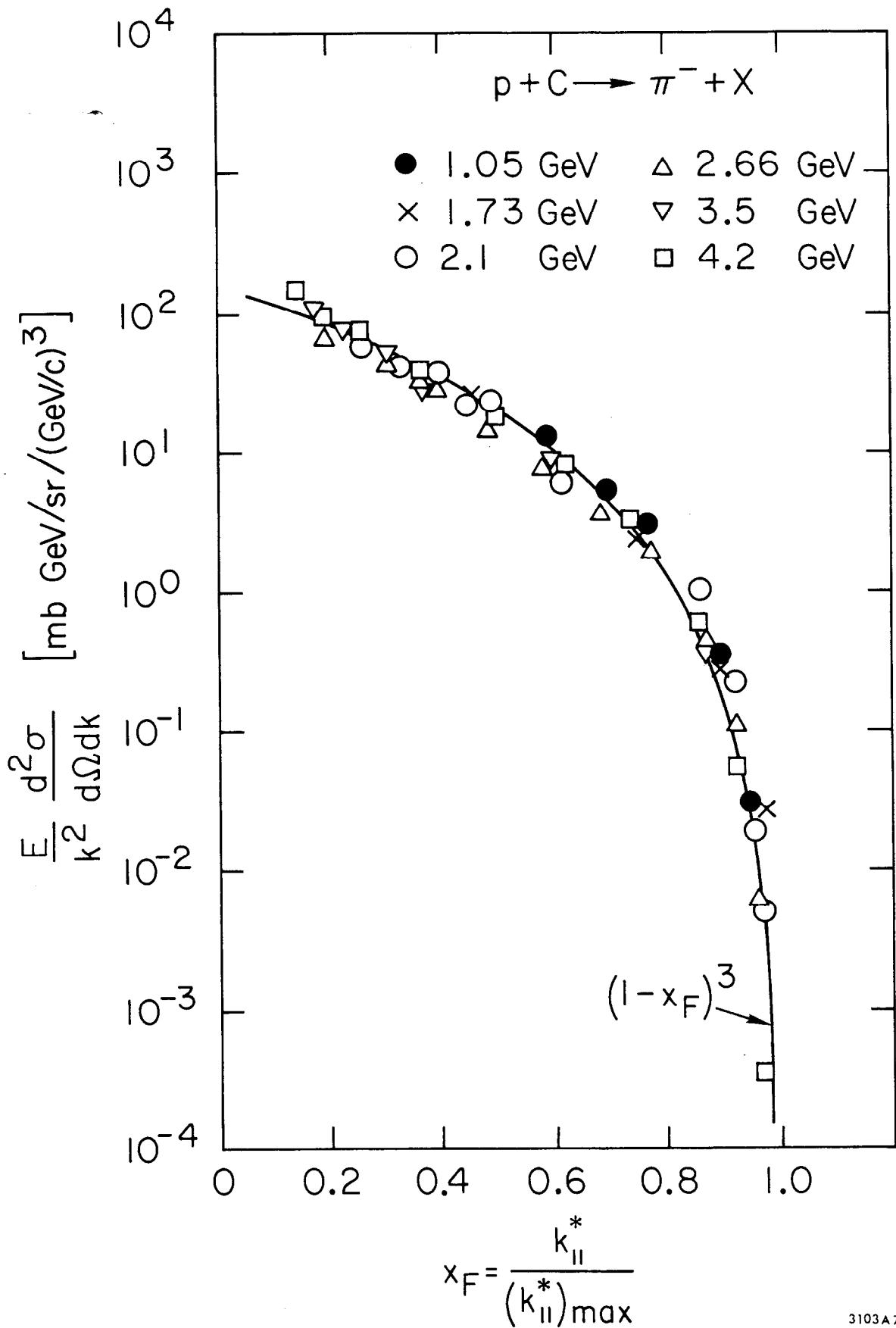
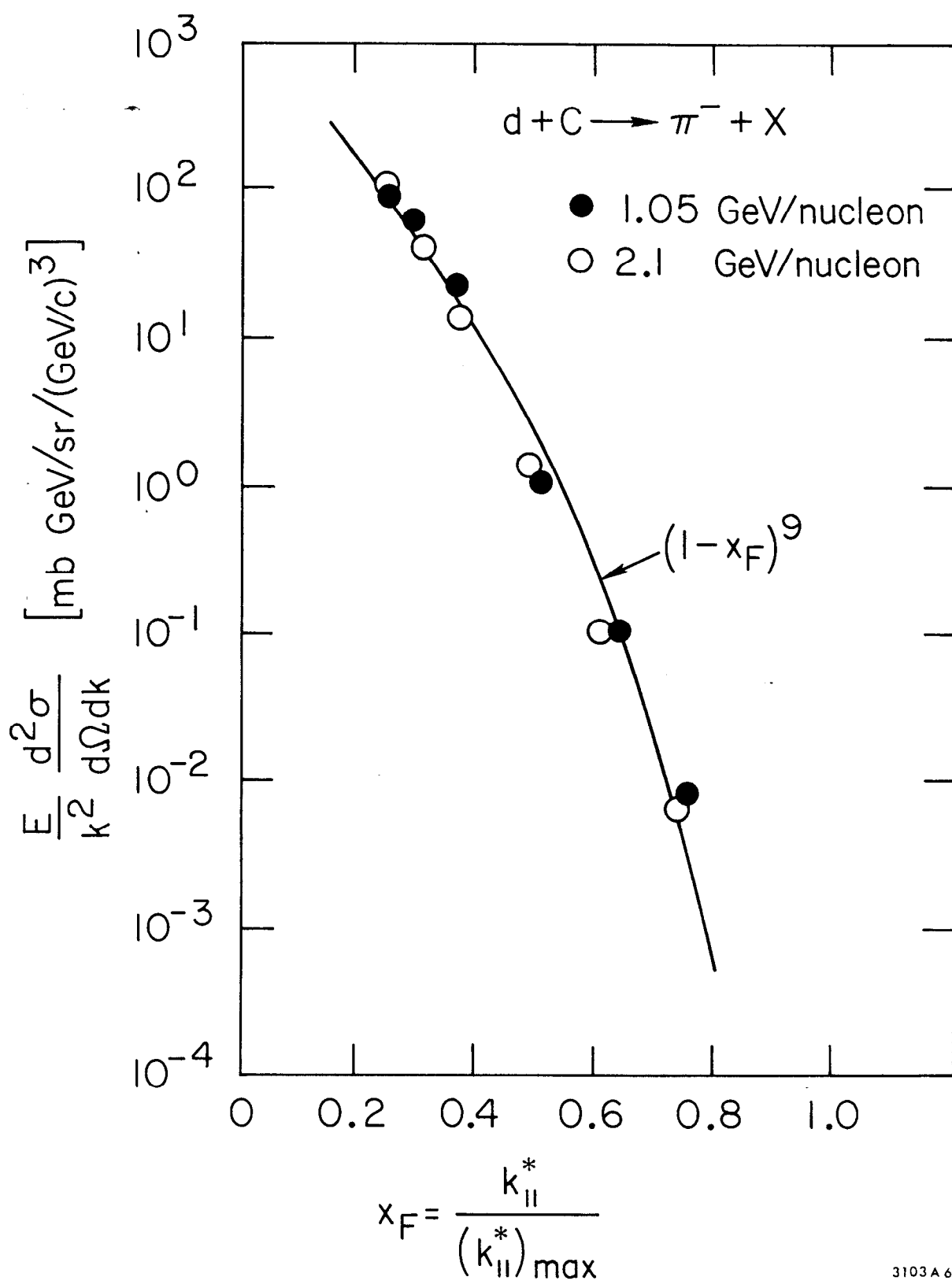
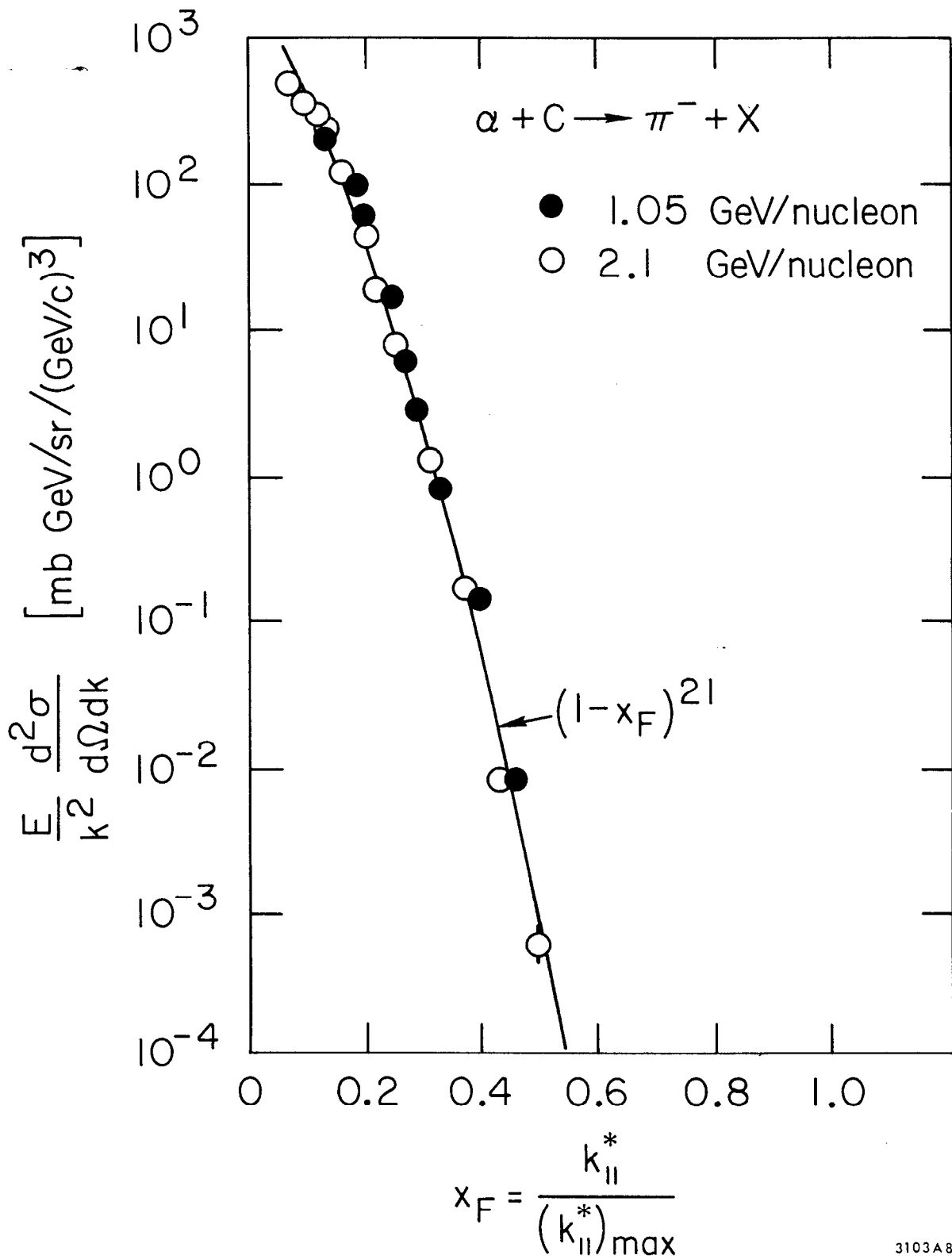


Fig. 4



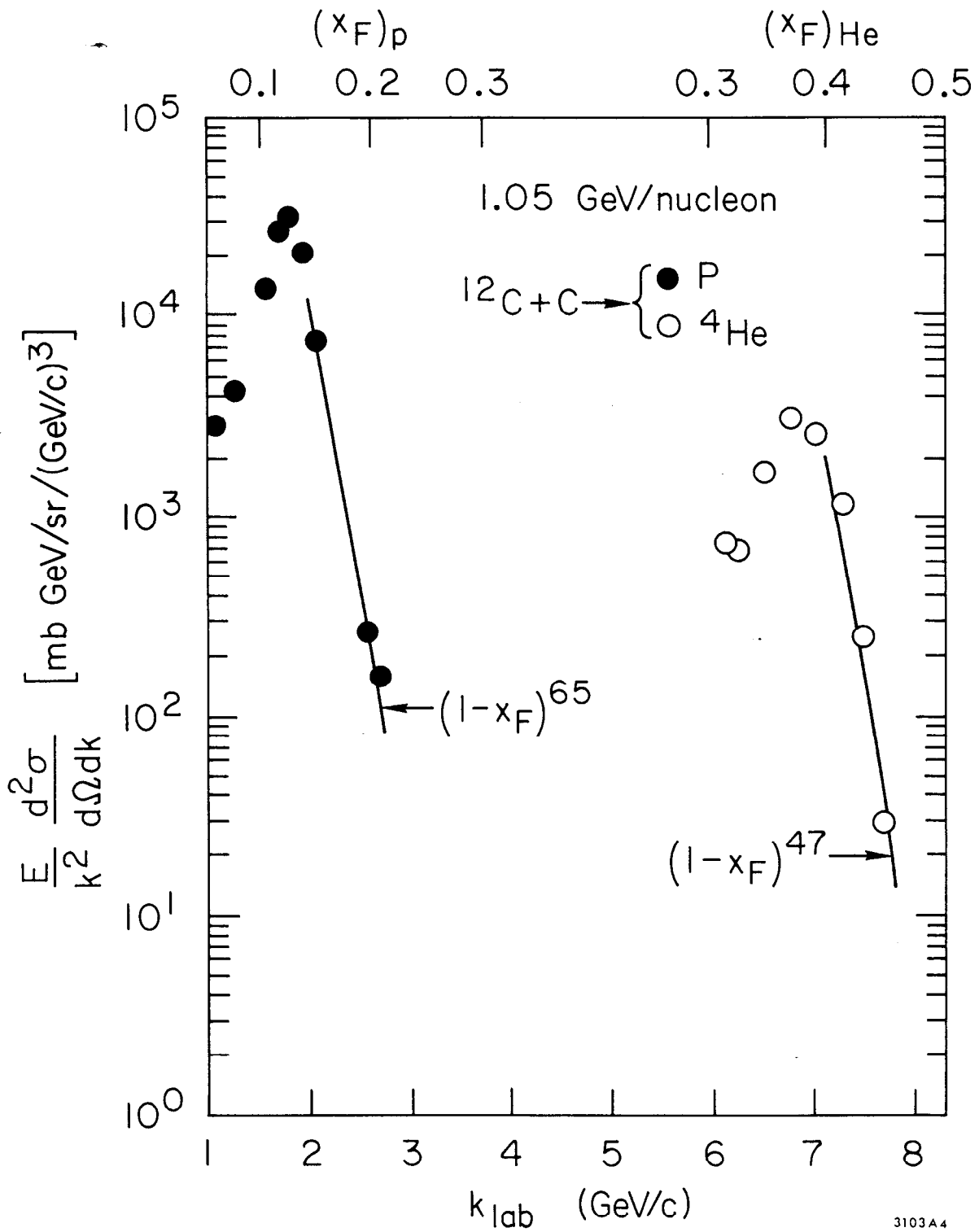
3103A6

Fig. 5



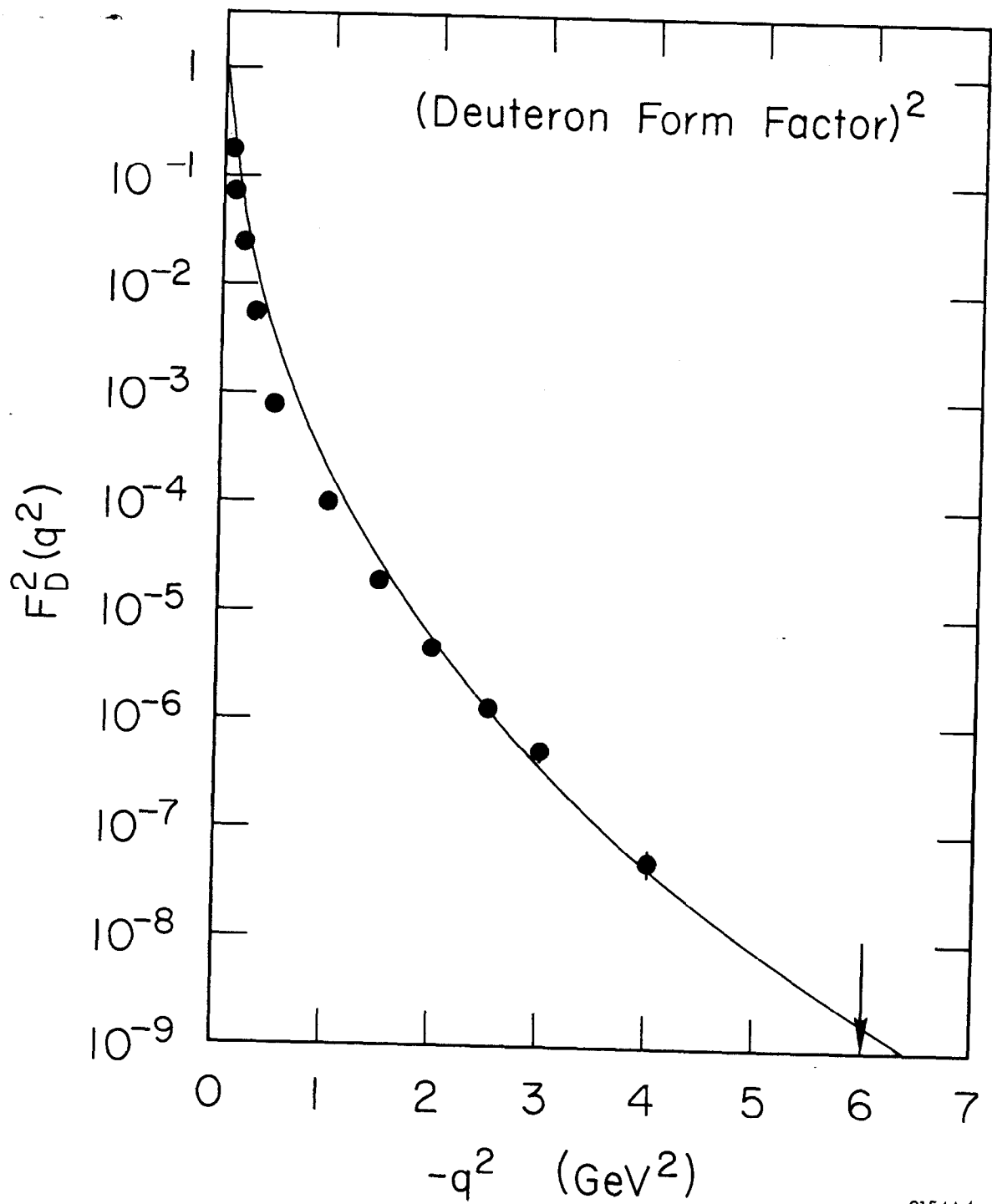
3103A8

Fig. 6



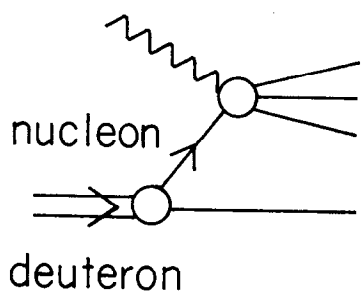
3103A4

Fig. 7



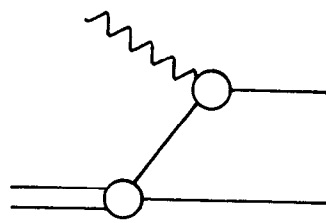
3154A4

Fig. 8

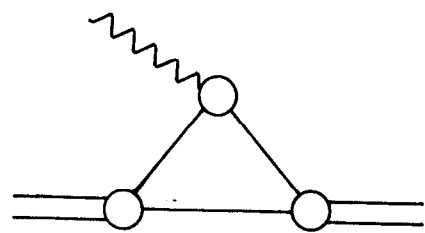


7-77

(a)



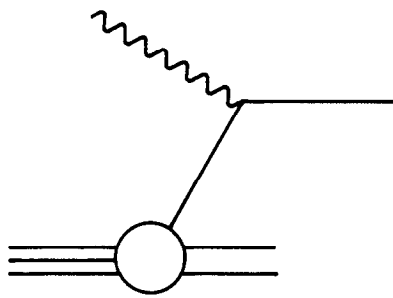
(b)



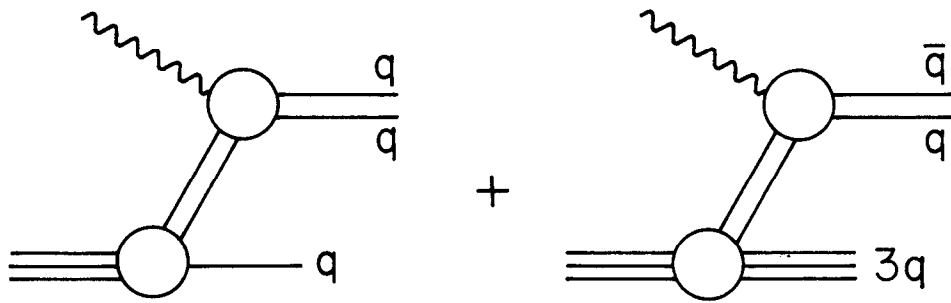
(c)

3239A7

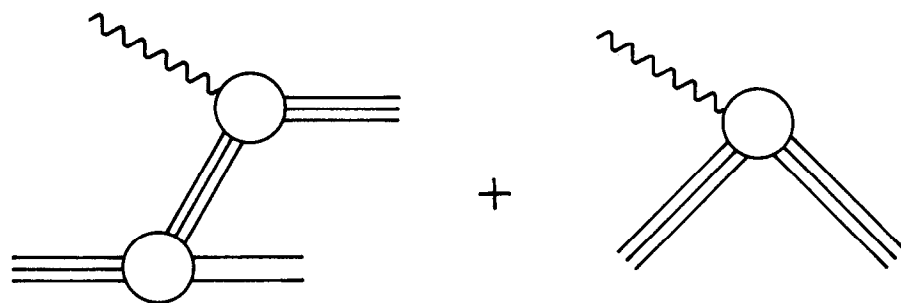
Fig. 9



(a)



(b)



(c)

3154A1

Fig. 10

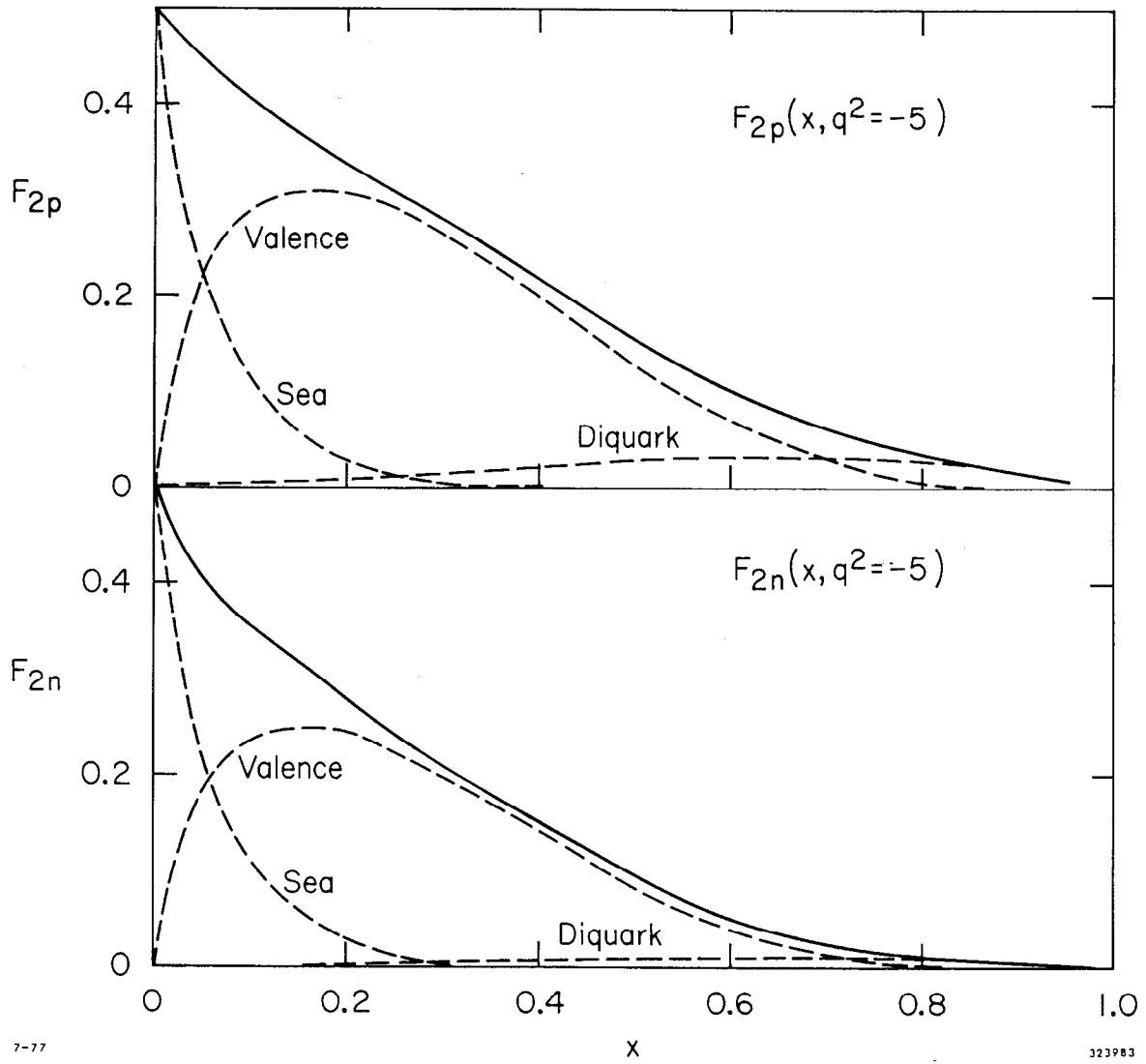
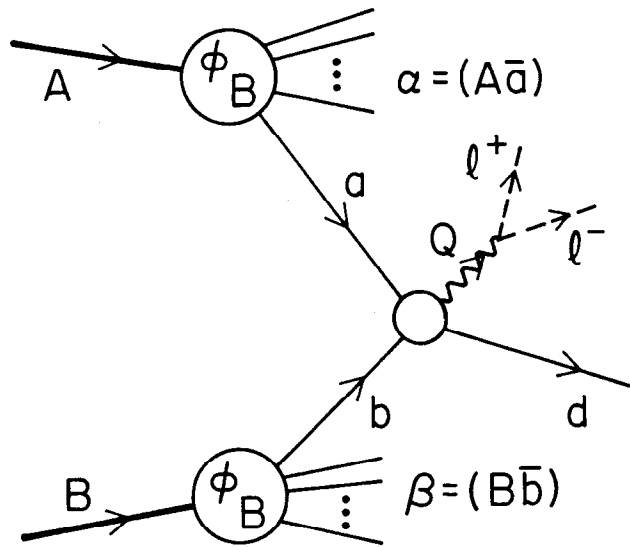
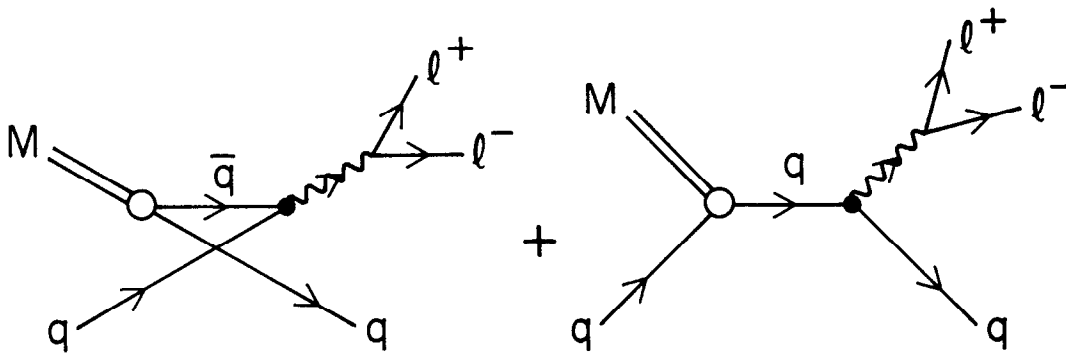


Fig. 11



(a)



(b)

9-77

3278A9

Fig. 12

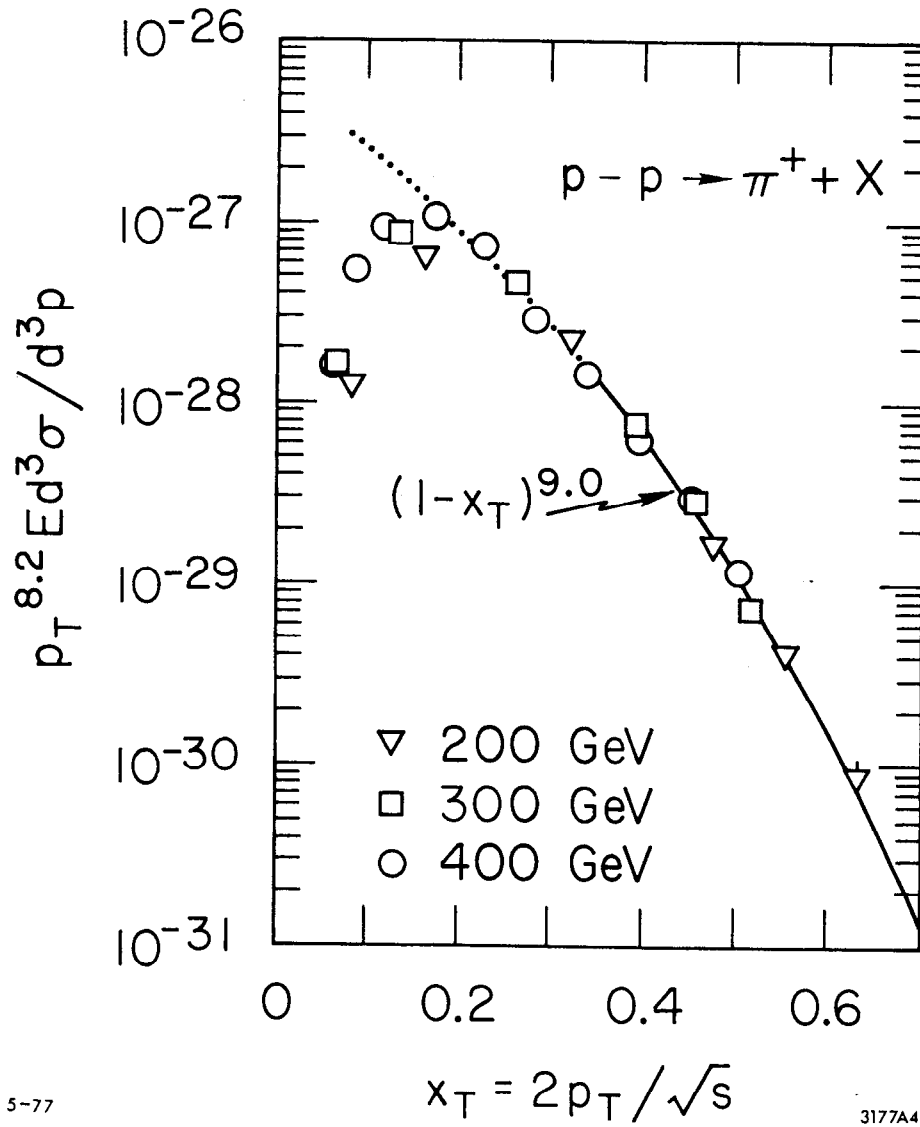
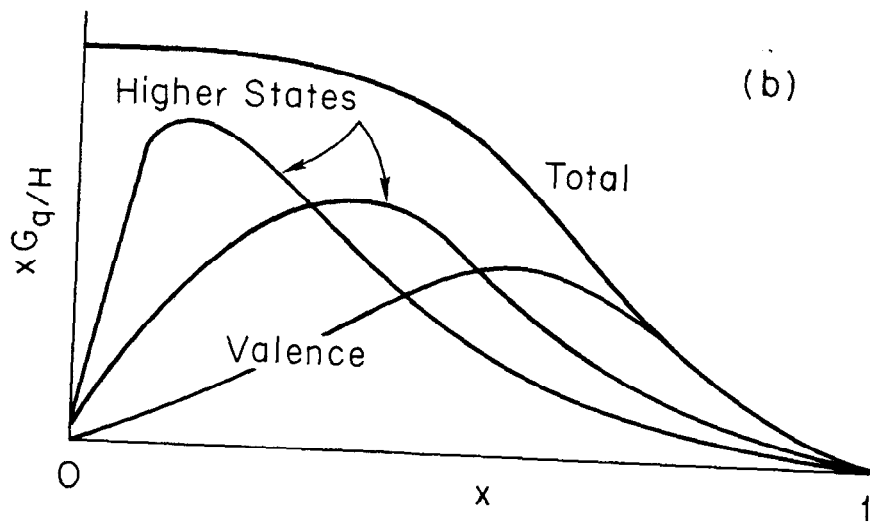
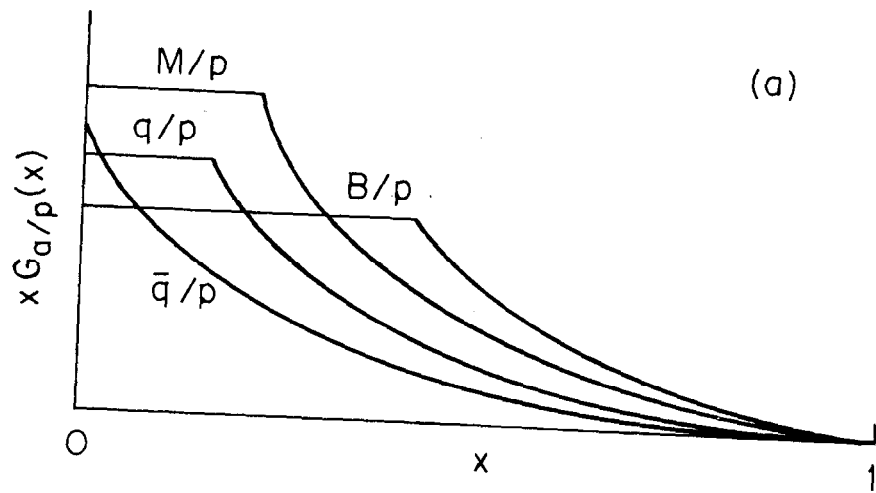


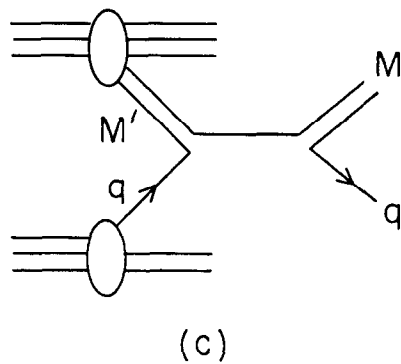
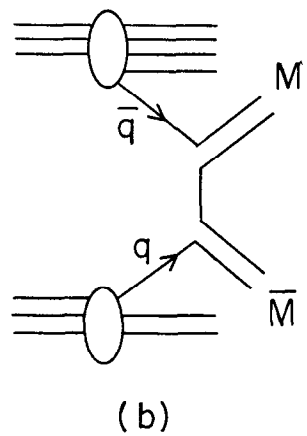
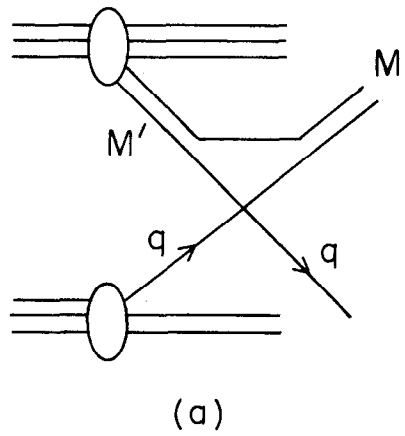
Fig. 13



10-77

3303A1

Fig. 14



11-77

3303A7

Fig. 15

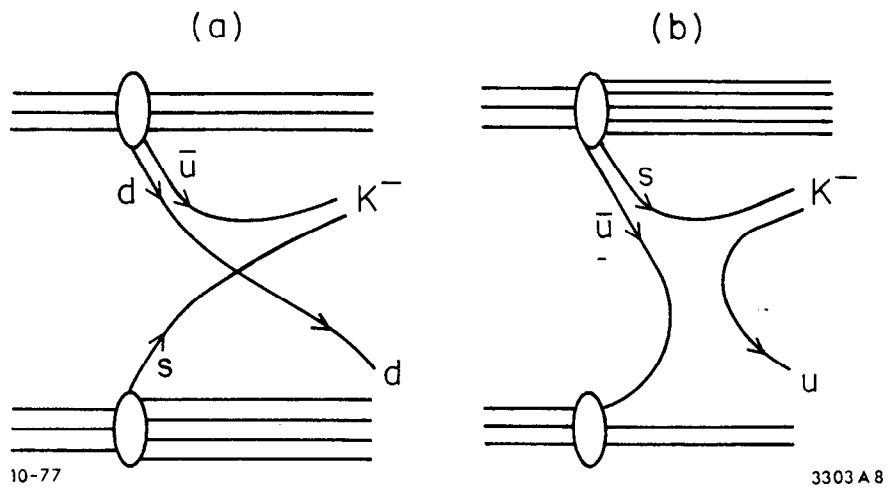
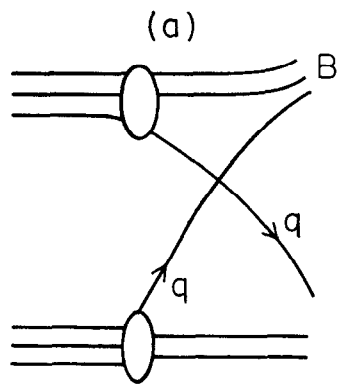
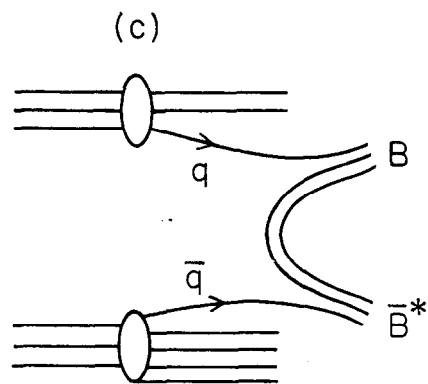
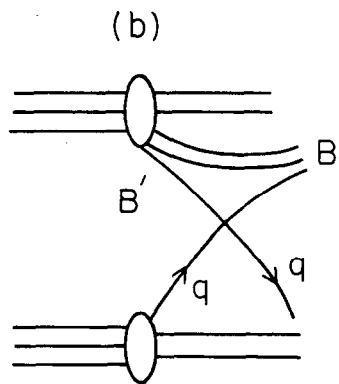


Fig. 16

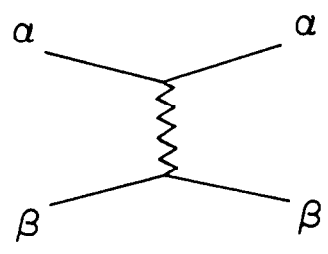


10-77



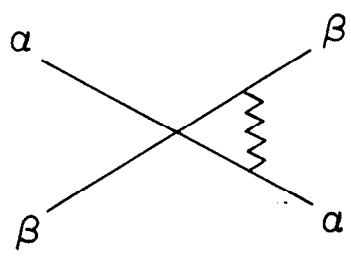
3303A9

Fig. 17



t-pole

10-77



u-pole

3303A13

Fig, 18'